Extratropical transition of tropical cyclones in a multiresolution ensemble of atmosphere-only and fully coupled global climate models

Article

Updated Version

It is advisable to refer to the publisher's version if you intend to cite from the work. See Guidance on citing.

www.reading.ac.uk/centaur

CentAUR

Central Archive at the University of Reading

Reading's research outputs online

Extratropical transition of tropical cyclones in a multiresolution ensemble of atmosphere-only and fully coupled global climate models

Alexander J. Baker[1,*], Malcolm J. Roberts[2], Pier Luigi Vidale[1], Kevin I. Hodges[1], Jon Seddon[2], Benoît Vannière[1], Rein J. Haarsma[3], Reinhard Schiemann[1], Dimitris Kapetanakis[3], Etienne Tourigny[4], Katja Lohmann[5], Christopher D. Roberts[6], and Laurent Terray[7]

[1] National Centre for Atmospheric Science and Department of Meteorology, University of Reading, Reading, Berkshire, UK

[2] Met Office Hadley Centre, Exeter, Devon, UK

[3] Koninklijk Nederlands Meteorologisch Instituut, De Bilt, The Netherlands

[4] Earth Sciences Department, Barcelona Supercomputing Center, Barcelona, Spain

[5] Max Planck Institut für Meteorologie, Hamburg, Germany

[6] European Centre for Medium-Range Weather Forecasts (ECMWF), Reading, UK

[7] Climat, Environnement, Couplages et Incertitudes, Centre Européen de Recherche et de Formation Avancée en Calcul Scientifique (CERFACS), Toulouse, France

* alexander.baker@reading.ac.uk

Corresponding author: Dr Alexander J. Baker

National Centre for Atmospheric Science
Department of Meteorology,
University of Reading
Earley Gate, Whiteknights Road, Reading, Berkshire RG6 6ES, UK
+44 (0) 118 377 762

1 **Abstract**

2 Tropical cyclones undergo extratropical transition (ET) in every ocean basin. Projected

3 changes in ET frequency under climate change are uncertain and differ between basins, so

4 multimodel studies are required to establish confidence. We used a feature-tracking algorithm

5 to identify tropical cyclones and performed cyclone phase-space analysis to identify ET in an

6 ensemble of atmosphere-only and fully coupled global model simulations, run at various

7 resolutions under historical (1950–2014) and future (2015–2050) forcing. Historical

8 simulations were evaluated against five reanalyses for 1979–2018. Considering ET globally,

9 ensemble-mean biases in track and genesis densities are reduced in the North Atlantic and

10 Western North Pacific when horizontal resolution is increased from ~100 to ~25km. At high

11 resolution, multireanalysis-mean climatological ET frequencies across most ocean basins as

12 well as basins' seasonal cycles are reproduced better than in low-resolution models. Skill in

13 simulating historical ET interannual variability in the North Atlantic and Western North

14 Pacific is ~0.3, which is lower than for all tropical cyclones. Models project an increase in ET

15 frequency in the North Atlantic and a decrease in the Western North Pacific. We explain

16 these opposing responses by secular change in ET seasonality and an increase in lower-

17 tropospheric, pre-ET warm-core strength, both of which are largely unique to the North

18 Atlantic. Multimodel consensus about climate-change responses is clearer for frequency

19 metrics than for intensity metrics. These results help clarify the role of model resolution in

20 simulating ET and help quantify uncertainty surrounding ET in a warming climate.

21

1. Introduction

The impacts of tropical cyclones are not confined to the tropics. Their post-tropical evolution makes these storms an important natural hazard across the midlatitudes (Baker et al., 2021; Bieli et al., 2019; Evans et al., 2017; Jones et al., 2003; Keller et al., 2019). The poleward propagation of tropical cyclones and the occurrence of extratropical transition (ET) exposes populous regions where risks to life and infrastructure are high—Northeast United States, maritime and eastern Canada, Western Europe, and East Asia—to hurricane-force wind speeds and extreme precipitation (Evans et al., 2017). In the North Atlantic, tropical-origin systems reached Northeast North America and Europe almost every year since 1979 (Baker et al., 2021), including recent intense landfalls. For instance, Hurricane Sandy (22nd–29th October, 2012)—the fourth costliest (by inflation-adjusted losses) North Atlantic hurricane yet recorded (Weinkle et al., 2018)—caused devastation across the Northeast United States and eastern Canada (Blake et al., 2013). Ex-hurricane Ophelia (9th–15th October, 2017) led to loss of life and severe wind damage across Ireland, the United Kingdom, and Scandinavia (Rantanen et al., 2020; Stewart, 2018). At midlatitude landfall, both systems were post-tropical, having begun ET, but possessed hurricane-like intensities, the human and economic impacts of which were felt across substantial areas. In the Western North Pacific, Typhoon Nabi (29th August–12th September, 2005) impacted two thirds of Japan's prefectures as both a tropical and transitioning cyclone before undergoing cyclolysis over Alaska (Harr et al., 2008). These events, along with the current lack of consensus regarding ET in a changing climate, heighten the urgency with which global studies of historical and near-future post-tropical cyclone activity are needed.

Tropical cyclones undergo ET in every ocean basin (Hart and Evans, 2001; Studholme et al., 2015; Wood and Ritchie, 2014; Zarzycki et al., 2017), but pronounced interannual variability (Baker et al., 2021) and basin-to-basin differences (Bieli et al., 2019) exist. Transitioning cyclones are also known to influence the large-scale circulation, such as Hurricane Debbie in 1982 (Laurila et al., 2019), and excite or amplify downstream Rossby waves (Evans et al., 2017; Jones et al., 2003; Keller et al., 2019; Michaelis and Lackmann, 2019). These cyclone-wave interactions influence downstream weather (Grams and Blumer, 2015; Keller et al., 2019). Of those cyclones which undergo ET, an appreciable proportion reintensify under favourable environmental conditions, where appropriate phasing between the transitioning cyclone and the upper-tropospheric flow pattern enhances baroclinic instability (Keller et al.,

55   2019). During and after ET, baroclinicity (Evans et al., 2017) and diabatic heating (Rantanen

56   et al., 2020) may reintensify the post-tropical cyclone.

57

58   Over the period of 1979–2018, statistically significant positive trends in the frequency of

59   North Atlantic ET events exist in several, but not all, reanalysis datasets (Baker et al., 2021).

60   Existing climate model projections underline the plausibility of increased tropical and post-

61   tropical cyclone activity in the midlatitudes in response to anthropogenic warming. There is

62   evidence that more frequent ET events may occur in the future in the North Atlantic (Baatsen

63   et al., 2015; Haarsma et al., 2013; Liu et al., 2017; Michaelis and Lackmann, 2019) and

64   Western North Pacific (Bieli et al., 2020) ocean basins, but no consensus yet exists across

65   studies, modelling campaigns, and methodologies. Moreover, best-track data limitations,

66   which are well documented (Chang and Guo, 2007; Delgado et al., 2018; Hagen et al., 2012;

67   Vecchi and Knutson, 2008), engender substantial uncertainty in observed trends (Lanzante,

68   2019; Moon et al., 2019). Additionally, natural, multidecadal variability in tropical-cyclone

69   frequency is yet to be accounted for (Knutson et al., 2020). Although global climate models

70   project reduced frequencies of tropical cyclones, more intense tropical cyclones are expected

71   in response to twenty-first-century warming (Knutson et al., 2020), potentially allowing a

72   higher proportion of cyclones to survive cooler midlatitude sea-surface temperatures

73   experienced prior to and during ET (Michaelis and Lackmann, 2019). Other factors,

74   particularly changes in shear, will also be important, with current evidence suggesting that

75   these will undergo ET-favourable future changes (Jung and Lackmann, 2021; Liu et al.,

76   2017; Michaelis and Lackmann, 2021). Increased future ET event frequency is also

77   consistent with the projected expansion of tropical-cyclone genesis regions (Studholme et al.,

78   2022), potentially reducing the mean displacement cyclones must undergo prior to

79   midlatitude ET. Together, these changes imply an increase in post-tropical cyclone impacts

80   across populated midlatitude regions, and idealised experiments suggest an increase in ET-

81   related, high-impact weather across Europe (Jung and Lackmann, 2021), where our

82   understanding of historical risks is developing (Baker et al., 2021). Studies of historical and

83   future model simulations are therefore needed to assess both contemporary risk and future

84   changes more comprehensively.

85

86   One aspect of climate model evaluation important for both tropical and extratropical cyclones

87   is understanding the role of horizontal resolution in simulated climates, prompted by recent

88   developments in high-performance computing and data-management facilities. With

89   increases in model resolution to approximately 25 km, improved fidelity is anticipated for

90   many synoptic phenomena, particularly tropical and midlatitude cyclones, which ultimately

91   feed back onto the large scale. Recent studies have now firmly established that increasing

92   model resolution improves simulated tropical-cyclone frequency statistics across most ocean

93   basins (Manganello et al., 2019; Roberts et al., 2020a), leads to a more realistic global spatial

94   distribution (Roberts et al., 2020a; Roberts et al., 2015; Strachan et al., 2013), and results in

95   more realistic simulated warm-core vertical structures (Vannière et al., 2020). Moreover,

96   model resolution is a key constraint on the intensity which simulated cyclones may reach

97   (Davis, 2018). It is anticipated that atmospheric resolutions of ~50 km or finer (~0.25 °

98   ocean-model resolution) will yield improvement in the simulation of post-tropical cyclones

99   and ET (Haarsma, 2021). However, no systematic multimodel studies of ET have been

100   undertaken, and the impact of increasing model resolution (atmosphere and ocean) on

101   simulated ET is also yet to be quantified. We address these issues in this paper using model

102   simulations from the 6th phase of the Coupled Model Intercomparison Project (CMIP6),

103   which follow an experimental protocol designed to isolate the impacts of changes in model

104   resolution.

105

106   In this study of the representation of tropical cyclones undergoing ET across a multimodel

107   ensemble, we focus on climatological statistics, interannual variability, and cyclone structure

108   and intensity. These analyses are centred around two questions. What is the impact of

109   increasing model atmospheric resolution on simulated ET? What changes in ET metrics

110   under climate change are consistent across models? This paper continues in section 2 with a

111   description of the model and reanalysis data as well as the cyclone-tracking and analysis

112   methodologies. Our results are presented in section 3 and our conclusions are summarised,

113   with further discussion, in section 4.

114

115

116   **2. Data and methodology**

117   *2.1 Reanalysis data*

118   Tropical cyclone best-track datasets are not well suited to analysis of cyclones undergoing ET

119   because there are known heterogeneities within individual datasets (Barcikowska et al., 2012;

120   Chu et al., 2002; Kossin et al., 2007; Vecchi and Knutson, 2008, 2011), especially for storms'

121   post-tropical stages, under-counting biases (Chang and Guo, 2007; Delgado et al., 2018;

122   Hagen et al., 2012), and differences between operational centres' data-collection

123   methodologies (Hodges et al., 2017; Schreck III et al., 2014). We therefore evaluated model

124   simulations against five global reanalyses (Table 1): the European Centre for Medium-Range

125   Weather Forecasts' Interim Reanalysis (ERAI; Dee et al., 2011) and Fifth Reanalysis (ERA5;

126   Hersbach et al., 2020); the Japanese 55-year Reanalysis (JRA55; Kobayashi et al., 2015); the

127   National Aeronautics and Space Administration's Modern-Era Retrospective Analysis for

128   Research and Applications version 2 (MERRA2; Molod et al., 2015); and the combined

129   National Centers for Environmental Prediction Climate Forecast System Reanalysis and

130   Climate Forecast System version 2 dataset (NCEP; Saha et al., 2014)—the sole fully coupled

131   (atmosphere, ocean, land surface, and sea ice) reanalysis used herein. Between reanalyses,

132   differing forecast model formulations and resolutions (horizontal and vertical), as well as

133   data-assimilation schemes lead to differences in the representation of tropical-cyclone

134   vertical structure, which was examined by Hodges et al. (2017). Baker et al. (2021) found

135   that interannual variability in the number ET events is well correlated between reanalyses,

136   but the percentage of tropical cyclones undergoing ET agrees less well between reanalyses on

137   the interannual timescale. It is therefore necessary to consider multiple reanalyses as an

138   observation-based reference, against which models may be evaluated.

139

Reanalysis	Analysis period	Analysis grid	Model resolution (grid spacing)	Data assimilation	Sample sizes (n_{NH}, n_{SH})
ERAI	1979–2017	512x256	TL255L60 (80 km)	4D-Var.	35.4, 37.0
ERA5	1979–2018	1140x721	T639L137 (33km)	4D-Var.	40.4; 38.2
JRA55	1959–2014	288x145	TL319L60 (55 km)	4D-Var.	35.6; 44.3
MERRA2	1980–2017	576x361	Cubed sphere (50 km)	3D-Var. + GSI + IAU	35.7; 28.6
NCEP	1979–2016	720x361	T382L64 (38 km)	3D-Var. + GSI	36.2; 30.6

141

142   **Table 1.** Reanalyses. Atmospheric mesh spacing at 50 °N in units of km is given in brackets.

143   3(4)D-Var.: 3(4)D variational data assimilation; GSI: Grid-point Statistical Interpolation;

144   IAU: Incremental Analysis Update. The representation of tropical and post-tropical cyclones

145   in these reanalyses were evaluated by Hodges et al. (2017) and (Baker et al., 2021),

146   respectively. Annual-mean global sample sizes (cyclones year^{-1}) for all tropical cyclones

147   undergoing ET for each reanalysis are given as n_{NH}, n_{SH}.

148

2.2 The multiresolution PRIMAVERA model ensemble

150 We evaluated CMIP6 High-Resolution Model Intercomparison Project (HighResMIP;

151 Haarsma et al., 2016) historical and future atmosphere-only (Tier 1 and Tier 3, respectively),

152 including interaction with the land surface, and fully coupled (Tier 2) simulations from five

153 global climate models (Table 2): CNRM-CM6.1 (Voldoire et al., 2019), EC-Earth3P

154 (Haarsma et al., 2020), ECMWF-IFS (cycle 43r1; Roberts et al., 2018), HadGEM3-GC3.1

155 (Roberts et al., 2019; Williams et al., 2018), and MPI-ESM1.2 (Gutjahr et al., 2019). Each

156 model participated in the European Commission Horizon2020-funded project PRIMAVERA

157 (PRocess-based climate sIMulation: AdVances in high-resolution modelling and European

158 climate Risk Assessments; primavera-h2020.eu). Historical (1950–2014) and future (2015–

159 2050) atmosphere-only experiments are termed *highresSST-present* and *highresSST-future*,

160 respectively, and fully coupled experiments are termed *hist-1950* and *highres-future*,

161 respectively. Historical *highresSST-present* simulations were forced by HadISST2 daily sea-

162 surface temperature (SST) at a resolution of 0.25 ° interpolated to each model's grid (no

163 ocean mixed-layer model). Out to 2050, *highresSST-future* simulations were forced

164 according to Representative Concentration Pathway 8.5 (RCP8.5). (Use of RCP8.5 allowed

165 modelling centres to begin their model simulations before Shared Socioeconomic Pathways

166 scenarios became available.) In HighResMIP, future simulations were performed with all

167 models except ECMWF-IFS. The rate of projected sea-surface temperature (SST) warming

168 was derived from an ensemble mean of CMIP5, with interannual variability derived from the

169 historical period 1950–2014 (Haarsma et al., 2016).

170

171 Under the HighResMIP experimental protocol, minimal changes in model-tuning parameters

172 were made between low- and high-resolution integrations to ensure that resolution-sensitivity

173 studies were not confounded by substantial differences in model configurations between

174 resolutions (Haarsma et al., 2016). Between low- and high-resolution configurations, no

175 model-physics changes were made to the atmospheric components of CNRM-CM6.1 and

176 EC-Earth3P, but minor adjustments were made to a single parameter in ECMWF-IFS (related

177 to net surface energy balance), HadGEM3-GC3.1 (related to quasi-biennial oscillation

178 period), and MPI-ESM1.2 (related to numerical stability). For the ocean model in coupled

179 configurations, one key difference is the effects of mesoscale eddies are parameterised at low

180 resolution (~1 °) but partially resolved at high resolution (~0.25 °) (e.g., Roberts et al., 2018;

181 Roberts et al., 2019). For all models, shorter dynamical timesteps were used in the high-

182 resolution integrations to ensure numerical stability. The effective resolutions of the high-

183   resolution model configurations, measured by kinetic energy spectra, resolve synoptic-scale

184   dynamics (Klaver et al., 2020). Since this study concerns cyclone translation from the tropics

185   to the extratropics, resolutions are given as a model's regular mesh spacing at a latitude of 50

186   ° (Table 2). For convenience, we refer to resolutions nominally (i.e., 'low' or 'high') as well

187   as quantitatively, where necessary. A single ensemble member was analysed at each

188   resolution for both the atmosphere-only and fully coupled experiments.

189

Atmospheric model	Ocean model	Atmospheric dynamical core	Resolution nomenclature	Atmospheric resolution	Atmospheric mesh spacing
ARPEGE6.3	NEMO	Spectral (linear, reduced Gaussian)	LR; HR	TL127; TL359	142; 50 km
IFS cyc36r4	NEMO	Spectral (linear, reduced Gaussian)	LR; HR	TL255; TL511	71; 36 km
IFS cyc43r1	NEMO3.4	Spectral (cubic octahedral; reduced Gaussian)	LR; HR	Tco199; Tco399	50; 25 km
MetUM	NEMO	Grid point (SISL)	LM (LL); MM; HM (HH)	N96; N216; N512	135; 60; 25 km
ECHAM6.3	MPIOM1.63	Spectral (triangular; Gaussian)	HR; XR	T127; T255	67; 34 km

Model name	CNRM-CM6.1	EC-Earth3P	ECMWF-IFS	HadGEM3-GC3.1	MPI-ESM1.2

Table 2. The PRIMAVERA (HighResMIP) model ensemble. NEMO: Nucleus for European Modelling of the Ocean. MPIOM: Max Plank Institute Ocean Model. SISL: semi-implicit, semi-Lagrangian. For fully coupled simulations, the LL and HH configurations of HadGEM3-GC3.1 were also included; LL denoting low-resolution atmosphere and low-resolution (1 °) ocean and HH denoting high-resolution atmosphere and high-resolution (1/12 °) ocean. Atmosphere mesh spacing is given for 50 °N. Sample sizes for all tropical cyclones undergoing ET across this ensemble are given in Table 3. DOIs for each simulation are listed at primavera-h2020.eu/modelling/.

200   *2.3 Lagrangian tropical-cyclone tracking*

201   To identify and track the evolution of tropical cyclones, we used the objective feature-

202   tracking algorithm—TRACK—of Hodges (1995), a well-established tool for identifying

203   cyclones in reanalyses (Hodges et al., 2017) and model simulations (Roberts et al., 2020a).

204   The TRACK algorithm was applied to six-hourly relative vorticity, computed from the zonal

205   and meridional wind fields, which was vertically averaged over the 850-, 700- and 600-hPa

206   levels and spectrally filtered. (Upper-level vorticity is used in subsequent identification.)

207   Filtering to the T6–T63 spectral band removes both large, planetary scales (total

208   wavenumbers 0-5) and small-scale noise (total wavenumbers >63). Vorticity maxima

209   exceeding 0.5×10^{-5} s^{-1} (in the Northern Hemisphere; scaled by -1 in the Southern

210   Hemisphere) were identified, initialised into tracks using a nearest-neighbour approach, and

211   subsequently refined by minimising a cost function for track smoothness, subject to adaptive

212   constraints on track displacement and smoothness (Hodges, 1995, 1999). The use of

213   vertically averaged vorticity improves temporal coherence in instances where vorticity

214   maxima shift between levels (Hodges et al., 2017).

215

216   Cyclone-centred sampling of meteorological fields along cyclone tracks was performed to

217   detect warm-core structures and measure cyclone intensities, following Hodges et al. (2017).

218   For warm-core identification, the T63-truncated vorticity data on seven levels covering 850–

219   250 hPa were added to tracks by recursively searching for a vorticity maximum at each level

220   using the previous level's maximum as the starting point for a steepest-ascent maximization

221   applied to the B-spline-interpolated field. A search radius of 5 ° was used, centred on each

222   level's maximum. For the Southern Hemisphere, fields were scaled by -1. To quantify

223   cyclone intensity, mean sea-level pressure minima within a radius of 5 ° and 925-hPa and 10-

224   metre wind speed maxima within a radius of 6 ° of the storm centre were sampled from

225   reanalysis or model-output fields at their native, non-truncated resolutions. (All radii are

226   geodesic.)

227

228   Following Hodges et al. (2017), objective identification of tropical cyclones adhered to the

229   following criteria:

230   ▪ cyclogenesis equatorward of 30 °N

231   ▪ total cyclone lifetime must exceed two days

232   ▪ T63 relative vorticity at 850 hPa must exceed 6×10^{-5} s^{-1}

233   ▪ T63 relative vorticity centre must exist at each level between 850 and 250 hPa to

234   indicate a coherent vertical structure

235   ▪ T63 relative vorticity decrease with increasing height between 850 and 250 hPa by at

236   least 6×10^{-5} s^{-1} to indicate the presence of a warm core

237 The three T63 relative vorticity criteria must also be jointly attained for at least four

238 consecutive time steps (i.e., one day) over ocean only. Together, these criteria minimise

239 inclusion of spurious short-lived or relatively weak vorticity features. The same criteria were

240 used for each reanalysis and model simulation and across all ocean basins.

241

242 Crucial to our analyses, vorticity-based tracking and post-tracking identification of tropical

243 cyclones yields longer cyclone lifecycles (compared with central-pressure-based algorithms

244 and methodologies where identification is performed during tracking), which allows for

245 objective analysis of post-tropical storm evolution (Hodges et al., 2017). A comparison of

246 TRACK results with results from a different tracking algorithm, which does not capture the

247 full lifecycle, demonstrates this advantage of vorticity-based tracking (section S1.1; Fig. S1).

248 In addition, filtering gridded data to a common spectral truncation, rather than tuning the

249 cyclone-tracking algorithm to a given dataset, allows both inter-model and inter-resolution

250 comparisons that are not complicated by methodological differences (Hodges et al., 2017).

251 Applying TRACK to a reanalysis globally, as described here, identifies ~30,000 tropical

252 vortices per year. Of these, ~8,000 per year have a lifetime that exceeds two days and are

253 retained; of these, ~120 per year exhibit the warm-core structure of a tropical cyclone

254 (Vannière et al., 2020). Our study is based on recently published tropical cyclone track

255 datasets, derived using a consistent methodology (Roberts et al., 2020a; Roberts et al.,

256 2020b). Sample sizes for all tropical cyclones undergoing ET are given in Table 3. Finally,

257 spatial track statistics—track and genesis densities—were computed using spherical kernel

258 estimators, following Hodges (1996).

259

Model name	Atmosphere-only		Fully coupled	
	highresSST-present	*highresSST-future*	*hist-1950*	*highres-future*
CNRM-CM6.1	42.3, 52.0	41.0, 47.5	43.4, 45.8	40.1, 39.4
CNRM-CM6.1-HR	47.9, 55.9	46.7, 51.5	50.0, 49.6	46.8, 42.3
EC-Earth3P	19.2, 29.3	20.1, 28.9	19.9, 27.6	19.1, 24.0
EC-Earth3P-HR	30.1, 32.1	29.1, 29.4	26.6, 28.8	26.8, 27.8
ECMWF-IFS-LR	34.7, 41.6	n/a	29.6, 41.5	n/a
ECMWF-IFS-HR	39.8, 44.6	n/a	34.5, 41.7	n/a
HadGEM3-GC3.1-LL	n/a	n/a	28.4, 38.7	28.6, 36.3
HadGEM3-GC3.1-LM	36.3, 50.0	36.5, 50.7	n/a	n/a
HadGEM3-GC3.1-MM	60.1, 68.8	60.9, 65.0	55.0, 56.0	53.2, 53.4
HadGEM3-GC3.1-HM	63.8, 69.0	63.1, 64.6	58.1, 56.4	58.9, 54.3
HadGEM3-GC3.1-HH	n/a	n/a	63.4, 56.2	60.1, 52.9
MPI-ESM1.2-HR	10.5, 16.0	9.4, 14.5	11.4, 16.9	10.4, 15.5
MPI-ESM1.2-XR	10.1, 17.0	9.6, 15.0	11.1, 17.4	10.1, 14.9

260

261 **Table 3.** Annual-mean global sample sizes (cyclones year^{-1}) for all tropical cyclones

262 undergoing ET in each model simulation, given as n_{NH}, n_{SH}.

263

264 *2.4 Cyclone phase-space analysis*

265 The temporal evolution of cyclone structure, including identifying ET, is quantifiable by

266 analysis of a cyclone's thermal wind fields (Hart, 2003; Hart and Evans, 2001). So-called

267 cyclone phase-space analysis involves three parameters: the thermal axisymmetry of the

268 cyclone (B; Eq. 1) and the lower- (T_L; Eq. 2) and upper-tropospheric (T_U; Eq. 3) cyclone-

269 relative thermal winds. In this study, these parameters were computed using 6-hourly data for

270 all reanalyses and climate models. B is defined as:

271 $$B = h \left(\overline{Z_{600} - Z_{925}} \,|_R - \overline{Z_{600} - Z_{925}} \,|_L \right) \tag{1}$$

272 where $h = 1$ for the Northern Hemisphere and -1 for the Southern Hemisphere, Z_p is

273 geopotential height (m) at level p (isobaric; hPa), and R and L denote the right- and left-hand

274 semicircles, respectively, relative to the cyclone's displacement direction. In this study, we

275 followed the majority of previous research (Bieli et al., 2019; Bieli et al., 2020; Dekker et al.,

276 2018; Hart, 2003; Liu et al., 2017; Studholme et al., 2015) and defined thermal axisymmetry

277 (i.e., non-frontal) as $B < 10$ and asymmetry (i.e., frontal) as $B \geq 10$ m. To compute T_L and T_U

278 between isobaric surfaces, Hart (2003) used the slope of the linear regression between ΔZ and

279 $\ln p$ as the derivative of ΔZ relative to $\ln p$ to determine the mean ΔZ over a given pressure

280 range. However, to ensure consistency between phase-space parameters computed from

281 reanalyses and model output, and to account for the different pressure levels on which

282 reanalysis and model data are available, it was necessary to adopt a three-level procedure,

283 following recent studies (Bieli et al., 2019; Bieli et al., 2020; Liu et al., 2017; Studholme et

284 al., 2015). Here, T_L (925–600 hPa) and T_U (600–250 hPa) are defined as vertical derivatives

285 of the horizontal geopotential height gradient:

286 $$T_L \equiv -|V_T^L| = \left. \frac{\partial (\Delta Z)}{\partial \ln p} \right|_{925 \text{ hPa}}^{600 \text{hPa}} \tag{2}$$

287 $$T_U \equiv -|V_T^U| = \left. \frac{\partial (\Delta Z)}{\partial \ln p} \right|_{600 \text{hPa}}^{250 \text{hPa}} \tag{3}$$

288 where p is pressure and $\Delta Z = Z_{max} - Z_{min}$, where Z_{max} and Z_{min} are the maximum and minimum

289 geopotential height, respectively, at a given level within a 5 ° radius of the cyclone centre.

290 Positive T_L or T_U indicates the presence of a warm core in the upper or lower troposphere,

291 respectively; negative values indicate a cold core. A deep warm- or cold-core structure is

292 identified where T_L and T_U have the same sign. We performed phase-space analysis for all

293 reanalyses (section 2.1) and all PRIMAVERA models (section 2.2). In our analysis, cyclone

294 centres in reanalyses and model output are those identified objectively by TRACK, which

295   ensures dynamical consistency between cyclone positions and the geopotential height field.

296   This differs from Bieli et al. (2020), who centred reanalysis geopotential data on best-track

297   storm locations. The approach taken in our study avoids any potential inconsistencies

298   between reanalysis and best-track storm centres, which would need to be accounted for,

299   particularly at weaker intensities (Hodges et al., 2017).

300

301   Among existing studies, various phase-space thresholds have been employed to identify ET

302   (e.g., Bieli et al., 2019; Hart and Evans, 2001; Kofron et al., 2010; Liu et al., 2017; Zarzycki

303   et al., 2017). We defined ET onset as either cold-core development (i.e., $T_L < 0$) or

304   development of thermal asymmetry (i.e., $B \geq 10$), thereby allowing for either ET pathway. ET

305   completion is defined as the first occurrence of both $B \geq 10$ m and $T_L < 0$. These thresholds

306   are suitable for high-resolution gridded data (Michaelis and Lackmann, 2019) and are

307   supported by cluster analysis of observed ET events (Arnott et al., 2004). However, much of

308   the ET-identification literature has focussed on the North Atlantic, yet ET phase-space

309   pathways may differ between ocean basins (Bieli et al., 2019). To account for these

310   difficulties in our global study, ET was identified only where the completion criterion is

311   satisfied for at least four consecutive timesteps (i.e., one day). The use of this additional one-

312   day criterion identifies meaningful temporal changes in B and T_L and avoids counting any

313   spurious, high-frequency temporal variability in phase-space parameters as multiple core-

314   structure changes, following (Baker et al., 2021). An analysis of the sensitivity of ET location

315   to methodological choices is presented in section S1.2, showing a large spread in ET location

316   (Fig. S2). In this study, ET-completion latitude was identified after a warm-core structure

317   persisted for at least 2 days based on phase-space parameters (i.e., $T_L > 0$ and $T_U > 0$),

318   corresponding to '*w*' in Fig. S2. As such, sample sizes (Table 1 and Table 3) remain

319   unchanged. This method avoids false positives in ET identification arising from tropical

320   depressions and other weak, precursor systems (Bieli et al., 2020), and is therefore more

321   appropriate to analysis of ET location (see section S1.2 for details).

322

323

324   *2.5. Identifying post-ET reintensification*

325   Instances of post-ET reintensification were defined as a post-ET change in p_{min} of at least –4

326   hPa, a threshold that is based on published case studies (e.g., Zhu et al., 2018), but the

327   number of identified reintensification events is necessarily sensitive to this threshold. For

328   consistency, we applied a single threshold across all reanalyses and models; a higher

329 threshold will likely be appropriate for any future analysis of higher-resolution (i.e.,

330 convection-permitting) models. We used p_{min} to avoid any complications arising from inter-

331 model differences in how near-surface wind speeds are computed (e.g., related to surface

332 roughness).

333

334

335 *2.6 Eady growth rate*

336 Eady growth rate maxima (Eq. 4) were computed as (Hoskins and Valdes, 1990):

337 $$\sigma_{max} = 0.31 \frac{f}{N} \frac{\partial(u,v)}{\partial Z} \tag{4}$$

338 where f is the Coriolis parameter, N is the static stability parameter, Z is geopotential height,

339 and u and v are the zonal and meridional winds, respectively, which were used to compute

340 the magnitude of the horizontal wind (i.e., $\sqrt{u^2 + v^2}$). The vertical derivatives, $\partial(u,v)$ and ∂Z,

341 were computed between the 850- and 250-hPa levels using 6-hourly data.

342

343

344 **3. Results**

345 In each of the following sections, we present historical results and model evaluation followed

346 by analysis of projected future changes out to 2050.

347

348

349 *3.1 Spatial cyclone statistics*

350 We first present spatial track density patterns for tropical cyclones undergoing ET in

351 reanalyses and simulated across the PRIMAVERA ensemble. Reanalyses exhibit a high

352 degree of consistency for track density and demonstrate that tropical cyclones undergo ET in

353 all ocean basins. However, fewer ET events are identified over the Northern Indian Ocean

354 (Fig. 1a), where relatively low-latitude landfall either disrupts liminal ET events or averts

355 potential ET cases altogether, primarily via boundary-layer frictional effects (Bieli et al.,

356 2019). Overall, basins' climatological ET activity is proportional to their tropical cyclone

357 activity. The highest ET frequencies are identified in both the Western North Pacific and

358 South Pacific basins, with climatological mean values of ~12 cyclones year[-1]. The North

359 Atlantic is the most active basin for ET outside the Pacific, and comparably low activity

360 occurs across the South Atlantic and South Indian basins (Fig. 1a).
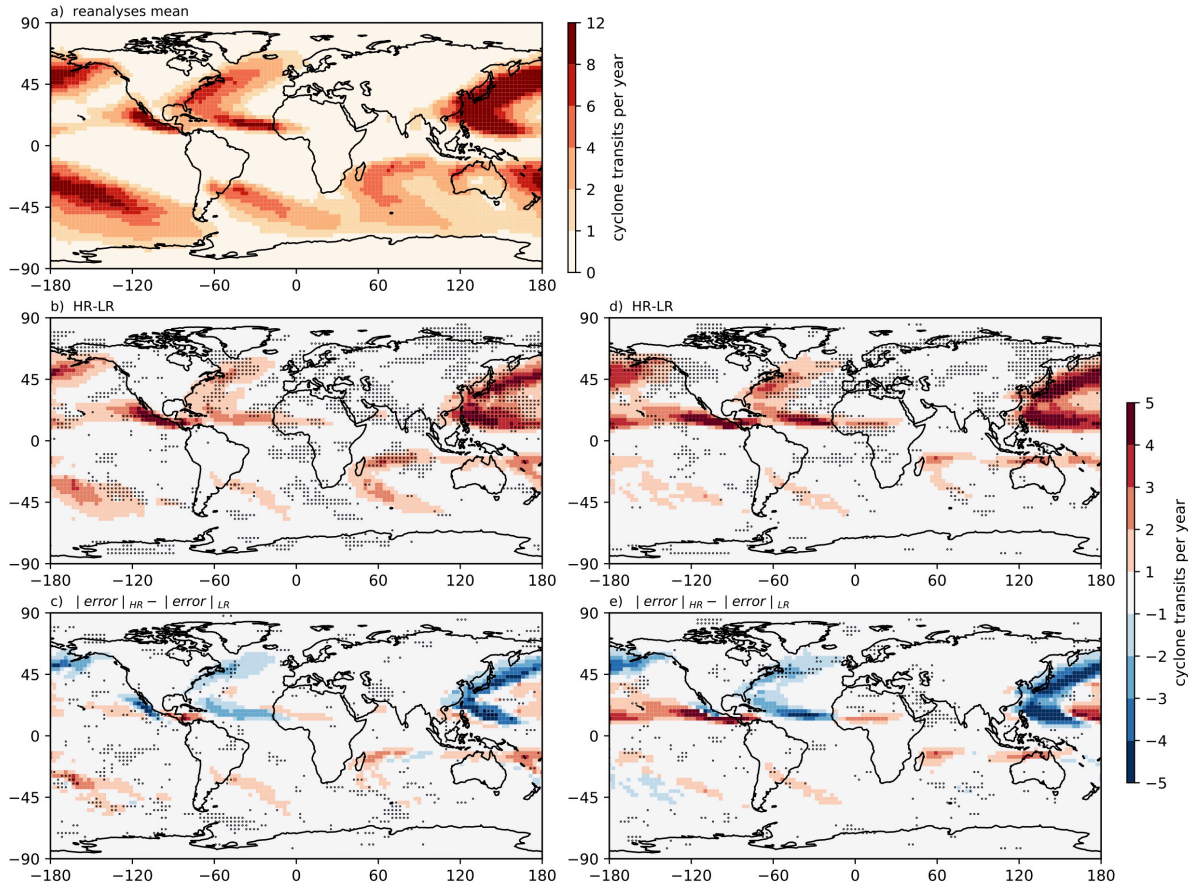
361

Fig. 1. Cyclone track density for all tropical cyclones undergoing ET. (a) Multireanalysis mean, (b–c) *highresSST-present* and (d–e) *hist-1950*. Track density was computed from complete tracks, including precursor stages, and is shown in units of cyclone transits per year per unit area (within a 5 ° geodesic radius of storm centres). All available reanalysis years (Table 1) are included in this analysis. (b, d) HR–LR denotes the ensemble-mean difference between high and low resolution. (c, e) |error|HR–|error|LR denotes the ensemble-mean difference of the absolute error (model versus multireanalysis mean) between high and low resolution. The low-resolution ('LR') sub-ensemble includes CNRM-CM6.1-LR, EC-Earth3P-LR, ECMWF-IFS-LR, HadGEM3-GC3.1-LM(-LL), and MPI-ESM1.2-HR. The high-resolution ('HR') sub-ensemble includes CNRM-CM6.1-HR, EC-Earth3P-HR, ECMWF-IFS-HR, HadGEM3-GC3.1-HM(-HH), and MPI-ESM1.2-XR. In b)–e), stippling indicates where all five models agree on the sign of the difference.

376   The frequency of ET events simulated by PRIMAVERA models increases when resolution is

377   increased from ~100 km to ~25km in all basins, both in the *highresSST-present* (Fig. 1b) and

378   *hist-1950* (Fig. 1d) experiments. Ensemble-mean climatologies are similar between both

379   experiments (Fig. S3). The North Atlantic and Western North Pacific basins are regions of

380   relatively widespread inter-model agreement on the sign of this resolution-sensitivity in track

381   density, again regardless of whether SST is prescribed. When prescribed, inter-model

382   agreement is also identified in the South Pacific and South Indian basins (Fig. 1b). This result

383   is consistent with a recent equivalent analysis of all tropical cyclones in PRIMAVERA

384   simulations (Roberts et al., 2020a), where increased frequencies were simulated at higher

385   model resolution across all ocean basins, for which the leading explanation is that finer

386   atmospheric resolution increases the conversion rate of precursor vortices (or 'seeds') to

387   tropical cyclones (Roberts et al., 2020a; Vecchi et al., 2019; Vidale et al., 2021). Tropical-

388   cyclone intensities simulated at model resolutions in the range 50–20 km are more

389   comparable with observational estimates (Roberts et al., 2020a), due in part to enhanced

390   surface latent heat flux (Vannière et al., 2020), implying that a more realistic proportion may

391   withstand midlatitude environmental conditions hostile to tropical cyclones prior to and

392   during the initial stages of ET. At low resolutions (typically ~100 km), PRIMAVERA models

393   simulate too few ET systems compared with reanalyses, particularly across the North Atlantic

394   and Western North Pacific, in both the *highresSST-present* (Fig. S4a) and *hist-1950* (Fig.

395   S4c) experiments. Increasing resolution to ~25 km leads to increased track density globally,

396   reducing negative biases in these basins but engendering positive biases in the Eastern North

397   Pacific and South Pacific (Fig. S4c, d). In *hist-1950*, this bias reduction is consistent with a

398   reduction in negative surface temperature biases at high resolution (e.g., ~1 ºK reduction in

399   the North Atlantic; Moreno-Chamarro et al., 2022). In section 3.2, we examine ET frequency

400   and the percentage of tropical cyclones undergoing ET separately.
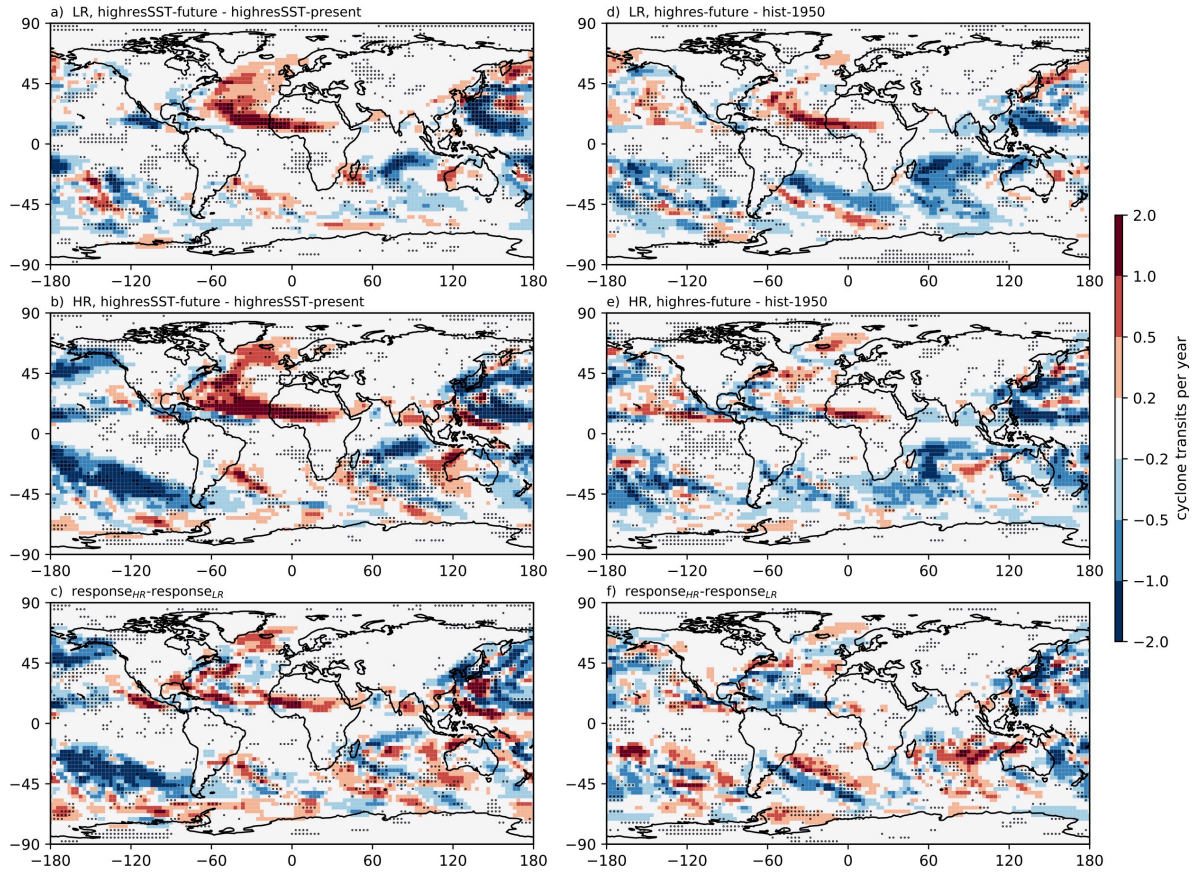
401

Fig. 2. Climate-change response of track density for all cyclones undergoing ET. (a–c) *highresSST-future* minus *highresSST-present* and (d–f) *highres-future* minus *hist-1950*. Track density was computed from complete tracks, including precursor stages, and is shown in units of cyclone transits per year per unit area (within a 5 ° geodesic radius of storm centres). The low-resolution ('LR') sub-ensemble includes CNRM-CM6.1-LR, EC-Earth3P-LR, HadGEM3-GC3.1-LM(-LL), and MPI-ESM1.2-HR. The high-resolution ('HR') sub-ensemble includes CNRM-CM6.1-HR, EC-Earth3P-HR, HadGEM3-GC3.1-HM(-HH), and MPI-ESM1.2-XR. Stippling indicates where all models agree on the sign of the difference.

412   Overall, PRIMAVERA simulations indicate that increasing resolution improves the

413   representation of ET frequency, as measured by track density, particularly across the North

414   Atlantic and Western North Pacific (Fig. 1c, e). For these basins, reductions in ensemble-

415   mean absolute biases are found in both *highresSST-present* and *hist-1950*, and areas of bias

416   reduction across multiple models occur primarily over western boundary currents—the Gulf

417   Stream and Kuroshio, respectively. That these regions of resolution-dependence and reduced

418   biases overlap indicates that capturing the sharpness of SST fronts and associated

419   baroclinicity is important in simulating ET (Evans et al., 2017; Klein et al., 2002), and,

420   consistent with this, we find enhanced meridional SST gradients in both of these boundary-

421   current regions (Fig. S5). In the Southern Hemisphere, little difference in ensemble-mean

422   biases is found between resolutions, with a caveat that observational or reanalysis-based

423   climatologies for the Southern Ocean are themselves more uncertain (Hodges et al., 2017).

424   The PRIMAVERA ensemble provides evidence that atmospheric resolutions typical of

425   CMIP6 are too coarse to adequately capture basin-mean tropical-cyclone (Roberts et al.,

426   2020a) and ET statistics (this study). Increasing resolution to ~25 km partly addresses this

427   shortcoming.

428

429   The climate-change response of track density for tropical cyclones undergoing ET in high-

430   resolution simulations is basin-dependent, with differences between atmosphere-only and

431   fully coupled simulations also apparent. In *highresSST-future*, increased track density is

432   simulated across the North and South Atlantic (but decreased over the eastern United States)

433   and over the Maritime Continent; decreases are simulated over the Eastern and Western

434   North Pacific and South Indian basins; and an unclear, mixed response characterises the

435   North Indian Ocean (Fig. 2a–b). Inter-model agreement about the sign of these changes is

436   largely confined to cyclogenesis regions (e.g., equatorial West Africa) and over the Gulf

437   Stream and Kuroshio Current. In *highres-future* simulations, positive climate-change

438   responses are confined to the central and Eastern North Pacific. The spatial response pattern

439   over the North Atlantic—increased over central and eastern North Atlantic and decreased

440   along the United States' east coast—is similar between *highresSST-future* and *highres-future*,

441   but the magnitude of the response is reduced in the fully coupled simulations (Fig. 2d–f).

442   This spatial pattern is supported by recent projections, with increases particularly apparent in

443   the eastern North Atlantic (Liu et al., 2017), consistent with the projected eastward and

444   poleward expansion of cyclogenesis within this basin (Haarsma et al., 2013).

445

446 Increasing horizontal resolution has a localised effect on the climate-change response of track

447 density for ET (Fig. 2c, f). In *highresSST-future*, resolution-sensitive responses to climate

448 change, which are common across *all* models, are seen only over the central North Atlantic

449 and parts of the Southern Ocean. In *highres-future*, spatially coherent and resolution-sensitive

450 responses to climate change are seen over the South Atlantic and Eastern North Pacific

451 basins, where simulated track density maxima are shifted equatorward at high resolution.

452 However, the spatial patterns of resolution sensitivity over the North Atlantic and Western

453 North Pacific broadly resemble the spatial climate-change response patterns, which indicates

454 that these responses are enhanced at high resolution in most models. This is seen more clearly

455 in the atmosphere-only experiment (Fig. 2c) than in the fully coupled experiment (Fig. 2f).

456

457

458 *3.2 Interannual variability in ET*

459 Over the period 1979–2018, high-resolution *highresSST-present* simulations reproduce the

460 multireanalysis-mean climatological ET counts for Northern Hemisphere basins (Fig. 3, left),

461 except for the Northern Indian Ocean, a basin where few ET events occur. However, little

462 improvement with increased resolution is seen for Southern Hemisphere basins (Fig. 3, left).

463 Again, uncertainty is higher across the Southern Ocean, with greater inter-reanalysis spread

464 seen for Southern Hemisphere basins. These results are also true of the *hist-1950* simulations

465 (Fig. 4, left). The *highresSST-present* simulations appear to capture decadal variability in the

466 role of SST in sustaining tropical cyclones to ET. In certain basins, periods are apparent

467 where the *highresSST-present* ensemble mean and multireanalysis mean ET count match

468 well: e.g., 1985–2000 for the North Atlantic and 1990–2005 for the Western North Pacific

469 (Fig. 3, left). These periods coincide with observed positive phases in Atlantic Multidecadal

470 Variability and Pacific Decadal Oscillation, respectively. For ET %, differences between

471 low- and high-resolution ensemble means are small for most basins (Fig. 3, right). This

472 suggests that the large-scale environmental conditions conducive to ET are not substantially

473 different across the range of model resolutions considered here. This indicates that increased

474 ET frequency at high resolution is driven primarily by increased tropical cyclone frequency,

475 not by an increase in ET %. Similar mean values and variance in ensemble-mean ET count

476 and ET % are simulated in both *highresSST-present* (Fig. 3) and *hist-1950* (Fig. 4)
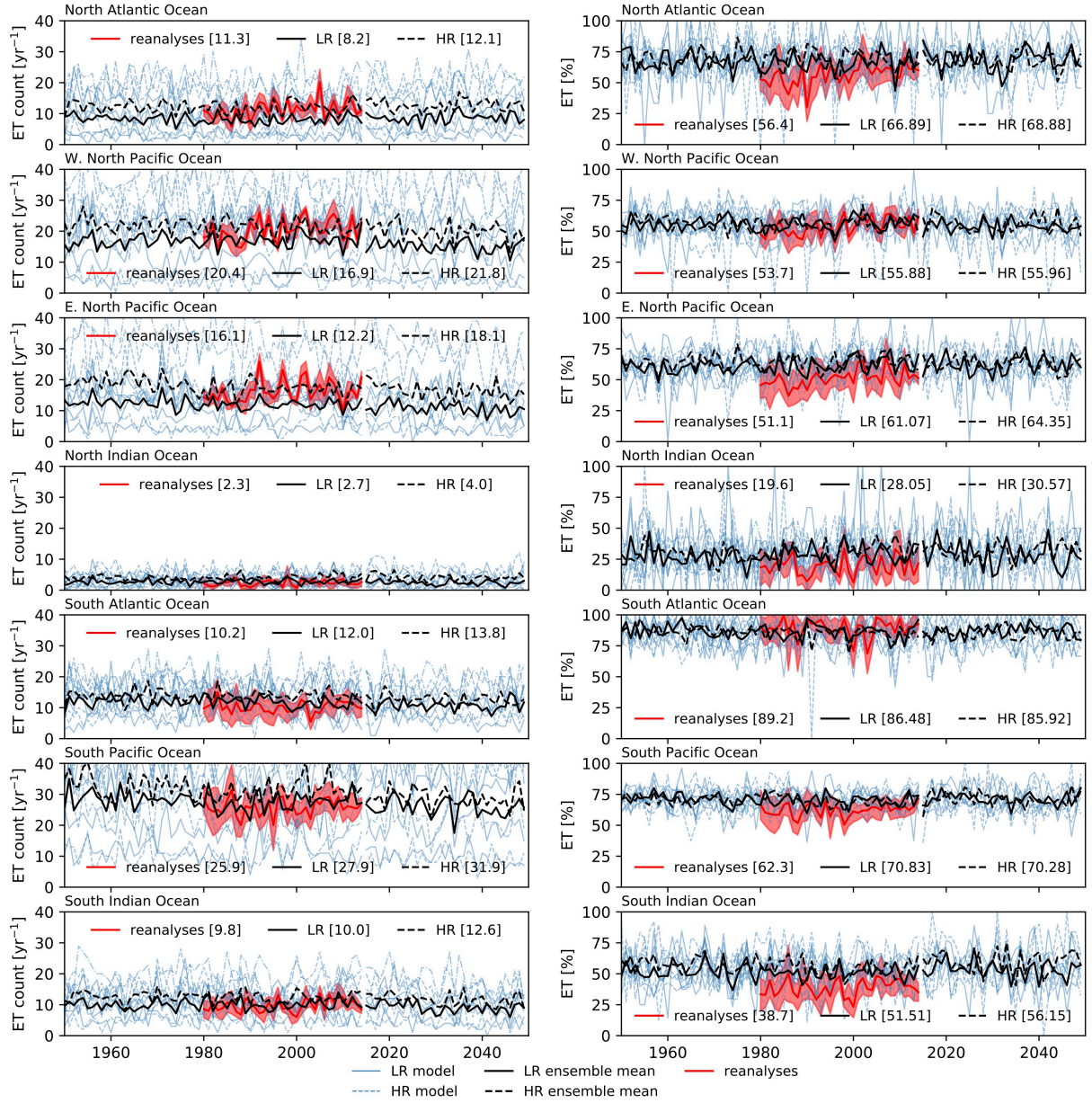
477 experiments.

478

479

Fig. 3. Interannual variability in (left) the number of ET events and (right) the percentage of tropical cyclones undergoing ET in each ocean basin in reanalyses and simulated in *highresSST-present* and *highresSST-future* experiments. Shown are (red) the multireanalysis mean, with 1 standard deviation of the reanalysis spread indicated by red shading, and (solid black) low- and (dashed black) high-resolution ensemble means. Each panel's legend gives climatological-mean values of (left) ET count or (right) ET % for the reanalyses and historical simulations. Also shown are (blue) timeseries for individual simulations to indicate the ensemble spread for each basin.

488

489   In *highresSST-present*, models' skill in reproducing the multireanalysis-mean interannual

490   variability in ET count varies between basins (Table 4). Interannual variability in ensemble-

491   mean and multireanalysis-mean ET counts are significantly, positively correlated for three

492   basins at low resolution and four basins at high resolution. The North Atlantic and Western

493   North Pacific basins are significantly correlated at both resolutions; the South Atlantic and

494   South Pacific basins are significantly correlated only at high resolution; and the Eastern

495   North Pacific is significant only at low resolution. Only for the North and South Indian basins

496   is ensemble-mean variability uncorrelated with reanalyses at either resolution. (Correlation

497   coefficients for *hist-1950* simulations are not shown because it is not expected that fully

498   coupled models' internal year-to-year variability would mimic that of forced simulations or

499   reanalyses.) For ET %, fewer significant correlations are found between ensemble-mean and

500   multireanalysis-mean timeseries (Table 4). Positive correlations are seen in the Northern and

501   Southern Indian basins and in the South Pacific basin at high resolution. However, low- and

502   high-resolution ensemble-mean ET % timeseries covary in most basins in both *highresSST-*

503   *present* (Fig. 3) and *hist-1950* (Fig. 4), more so than for ET count. To explain this, we

504   hypothesise that the large-scale environment conducive to the baroclinic conversion of

505   tropical cyclones is less sensitive to model resolution, while ET count depends on tropical

506   cyclone count, which is sensitive to model resolution (Roberts et al., 2020a).

507

508   Recent analysis of an ensemble of HadGEM3-GC3.1 simulations, performed under

509   HighResMIP, demonstrated that mean skill in representing interannual variability in tropical

510   cyclone count improves with additional members (Roberts et al., 2020a). At present, the

511   required six-hourly geopotential outputs are available for too few ensemble members to

512   repeat such an analysis for tropical cyclones undergoing ET, but this would constitute

513   valuable future work when sufficient model output is obtainable. Nonetheless, quantifying

514   the level of skill that exists in capturing interannual variability in the subset of tropical

515   cyclones that undergo ET, while lower than that for all tropical cyclones, is important,

516   establishing the baseline for HighResMIP-class models. This prompts further examination of

517   ET seasonality in the historical and future atmosphere-only simulations, which is possible in

518   the continuous PRIMAVERA simulations.

519

Ocean basin	ET count		ET %	
	LR	**HR**	**LR**	**HR**
North Atlantic	**0.31**	**0.30**	0.24	-0.16
Western North Pacific	**0.50**	**0.34**	0.21	0.24
Eastern North Pacific	**0.43**	0.22	**0.42**	0.16
North Indian	-0.08	0.03	0.03	**0.38**
South Atlantic	0.07	**0.34**	0.12	0.27
South Pacific	0.08	**0.50**	0.17	**0.34**
South Indian	-0.04	-0.19	0.24	**0.33**

520

521 **Table 4.** Pearson's *r* coefficients for correlations between low- (LR) or high-resolution (HR)

522 ensemble-mean and multireanalysis-mean interannual variability in ET count and ET % for

523 each ocean basin. Coefficients are shown only for *highresSST-present*; *hist-1950* simulations

524 are not shown because it is not expected that coupled models' internal year-to-year variability

525 would mimic that of forced simulations or reanalyses. Significant ($p < 0.1$) correlations are in

526 bold type.

527

528
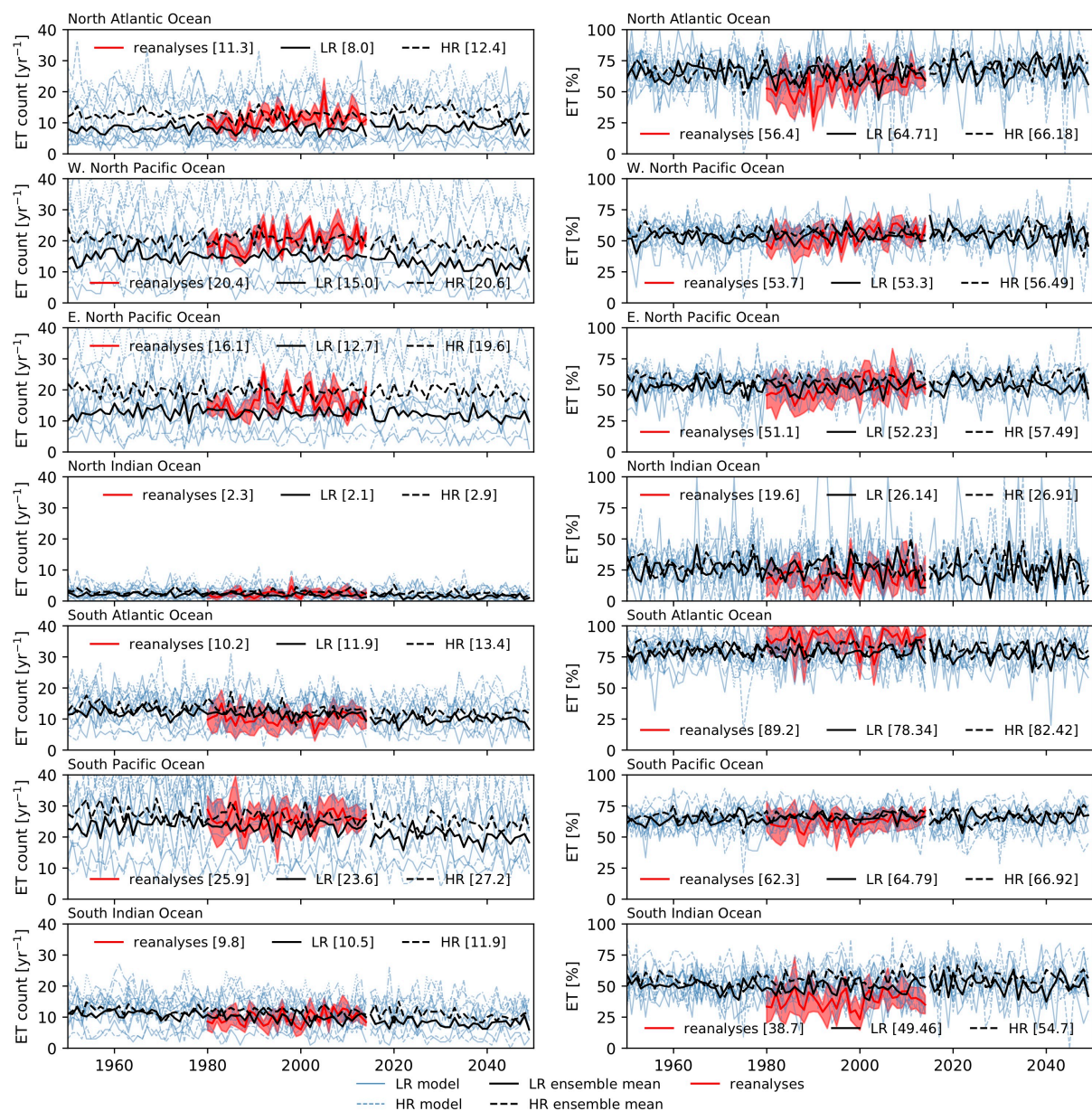
Fig. 4. As in Fig. 3 for fully coupled *hist-1950* and *highres-future* simulations.

530

531   *3.3 Historical and future ET seasonality*

532   We next evaluate the seasonal cycle of ET, focussing on the North Atlantic and Western

533   North Pacific basins for which both climatological ET statistics (Fig. 1) and interannual ET

534   variability (Table 4) are represented reasonably across models. In the North Atlantic,

535   reanalyses show ET % increasing from July to a peak in September before declining into

536   winter (Fig. S6a). In the *highresSST-present* experiment, most models reproduce this

537   seasonality, but the magnitude of the seasonal peak is overestimated by ~10 % at high-

538   resolution. There are indications that increased atmospheric resolution improves the

539   simulation of the timing of the seasonal ET % peak. Two models—CNRM-CM6.1 and EC-

540   Earth3P—simulate the seasonal peak too early (in August) at low resolution but simulate a

541   later peak (in September) at high resolution. Additionally, MPI-ESM1.2, the lowest-

542   resolution model in this ensemble, simulates comparably muted seasonality that also peaks

543   earlier than reanalyses at both resolutions. In the fully coupled *hist-1950* experiment, models

544   reproduce the multireanalysis-mean seasonal cycle, but HadGEM3-GC3.1 and CNRM-

545   CM6.1 simulate a broader seasonal distribution compared with reanalyses (Fig. S7a). In the

546   Western North Pacific, reanalyses show bimodal seasonality, with peaks in ET % in May and

547   September (Fig. S6b). Excepting the MPI-ESM1.2 model, which does not capture

548   bimodality, *highresSST-present* simulations also exhibit two seasonal peaks, but each occurs

549   one to two months later than in reanalyses in both low- and high-resolution integrations (Fig.

550   S6b), and this also holds true for *hist-1950* simulations (Fig. S7b).

551

552   To assess any potential future change in seasonality, ΔET %, we differenced the historical

553   and future seasonal cycles. For the North Atlantic, despite pronounced inter-model spread

554   throughout most of the annual cycle, there is an indication of more consistent model

555   behaviour during August–November, months for which most models simulate an increase in

556   ET % in both the *highresSST-future* (Fig. S6c) and *highres-future* experiments (Fig. S7c). To

557   quantify the degree to which this inter-model consistency represents secular change in ET

558   seasonality, the annual fraction of total annual ET events occurring during August–November

559   was computed. A significant, positive trend in this quantity over the period 1950–2050 is

560   found in the ensemble mean of high-resolution atmosphere-only simulations (Fig. 5a), but the

561   trend is not significant in reanalyses, which likely cover too short a period (1980–) to assess

562   secular change, and is significant in the low-resolution ensemble mean only at the 80 % level.

563   In fully coupled simulations, no significant trends are seen (Fig. S8a). Conducting a similar

564   analysis of the forthcoming extension of ERA5 back to 1950 is warranted, pre-satellite

565   observational uncertainty notwithstanding. For the Western North Pacific, the inter-model

566   spread during the annual cycle of ΔET % is similar between *highresSST-future* (Fig. S6d) and

567   *highres-future* simulations (Fig. S7d) and, in contrast to the North Atlantic, no significant

568   secular change in ET seasonality is found in either reanalyses or in PRIMAVERA

569   simulations out to 2050 (Fig. 5b and Fig. S8b). However, together with projected changes in

570   track density (Fig. 2a–b, d–e), these results provide further evidence that the future response

571   of ET to climate change across the North Atlantic differs from that of the Western North

572   Pacific and of other ocean basins. Therefore, we next investigate the role of cyclone structure

573   in explaining these distinct North Atlantic and Western North Pacific responses.
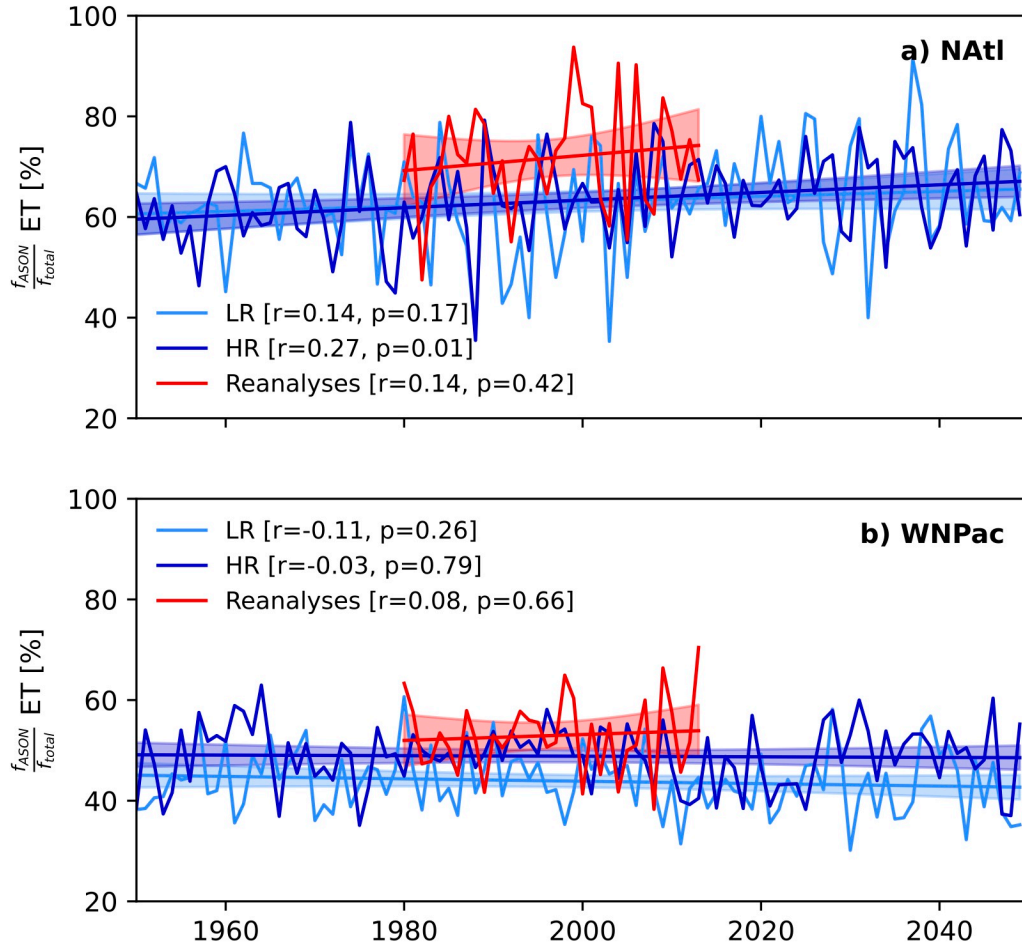
574

575

Fig. 5. Secular change in the proportion of ET events occurring during August–November in reanalyses (red) and low- (pale blue) and high-resolution (dark blue) atmosphere-only simulations (ensemble mean) for the (a) North Atlantic and (b) Western North Pacific basins. Shading shows the 95 % confidence interval for the linear fit. ECMWF-IFS is not included in this analysis because no future simulations were performed in HighResMIP for this model.

581

582   *3.4 Response of cyclone structures to climate change*

583   To examine the response of cyclone core structure to climate change, we computed

584   ensemble-mean bivariate frequency distributions of phase-space parameters, B, T_L, and T_U in

585   the high-resolution simulations. The T_L–B distribution exhibits a similar general structure in

586   the *highresSST-present* and *-future* experiments for both the North Atlantic (Fig. 6a–b) and

587   Western North Pacific (Fig. 6d–e) basins. This is also true for T_L–T_U distributions (Fig. 7a–b

588   and Fig. 7d–e). Generally, tropical cyclones undergoing ET occupy the lower-right

589   (symmetric, warm core) and upper-left (asymmetric, cold core) quadrants, with fewer

590   instances in either hybrid (transitional) quadrant. The phase-space parameter distributions

591   simulated across PRIMAVERA models are consistent with previous studies (Hart et al.,

592   2006; Michaelis and Lackmann, 2019). Historical ensemble-mean values of B and T_L for the

593   North Atlantic are consistent with recent analysis of observations (Studholme et al., 2015) as

594   well as reanalyses and Community Atmosphere Model simulations at resolutions of 55 and

595   28 km (Zarzycki et al., 2017). Ensemble-mean T_U values are also consistent with these

596   existing studies, except that deep warm-core structures are less frequent in PRIMAVERA

597   models than in recent 15-km-resolution simulations with the Model for Prediction Across

598   Scales–Atmosphere model (Michaelis and Lackmann, 2019), likely due to differences in

599   atmospheric resolution. For the Western North Pacific, model-simulated phase-space

600   parameters are consistent with reanalysis-based values (Kitabatake, 2011). In the fully

601   coupled simulations, T_L–B distributions for both basins are similar to those of the

602   atmosphere-only simulations (Fig. 8c, f), but differences in ensemble-mean T_U values are

603   seen, with warm-core responses to climate change occurring variously throughout the

604   troposphere (Fig. 9c, f).

605

606   Under climate change, models forced by prescribed SST simulate stronger warm-core

607   structures in the North Atlantic, indicated by a shift towards higher T_L for axisymmetric

608   tropical cyclones (Fig. 6c). Moreover, T_L–T_U distributions show that the future shift to

609   stronger warm-core structures is primarily confined to the lower troposphere (Fig. 7c, f).

610   (Here, 'strong' refers to ensemble-mean T_L values at the higher end of the historical

611   distributions, in which a range of model-simulated intensities are averaged.) These findings

612   are supported by a recent single-model study (Michaelis and Lackmann, 2019), albeit the

613   ensemble-mean signal we report is less pronounced, and are consistent with increased low-

614   level moisture and the potential for enhanced latent heat release in a warmer climate. Future

615   changes in core structures offer a partly mechanistic explanation of the projected increase in

616   ET across the North Atlantic (Baatsen et al., 2015; Haarsma et al., 2013; Liu et al., 2017) as

617   well as the projected change in track density, which is largely unique to the North Atlantic

618   (Fig. 2a–b, d–e). The lesser energy of weak warm-core cyclones is more likely to dissipate

619   before ET may occur, but relatively strong warm-core structures make cyclones more

620   resilient to unfavourable midlatitude environmental conditions (primarily cooler SST and

621   increased vertical wind shear), prolonging their poleward propagation and making ET more

622   probable across the North Atlantic (Hart et al., 2006).

623

624   In the North Pacific, however, this future shift to stronger warm cores is not seen in

625   PRIMAVERA models (Fig. 6f), although more frequent asymmetric, warm-core hybrid

626   structures (upper-right quadrant) in the future are simulated. These instances of hybrid

627   structures show cyclones existing more frequently in the transitional quadrants, potentially

628   indicating a future elongation of ET time (Zarzycki et al., 2017) and an increase in warm-

629   seclusion occurrences, which involve multiple transitions (Baker et al., 2021; Dekker et al.,

630   2018). Also seen is a shift towards stronger upper-level, cold-core structures (Fig. 7f). The

631   Western North Pacific is therefore characterised by more mixed future changes in core-

632   structure frequencies, consistent with the projected response of track density, which generally

633   decreases across the basin but increases in localised areas (Fig. 2b, e). Broadly, these results

634   are also consistent with the lack of any consensus in published projections of ET frequency

635   across the Western North Pacific: both a less favourable future ET environment (Ito et al.,

636   2016) versus moderate future increase in ET frequency (Bieli et al., 2020) have been

637   suggested. For both basins, future phase-space changes in the fully coupled simulations

638   resemble those seen in the atmosphere-only experiments, but the North Atlantic climate-

639   change signal is comparably muted (Fig. 8c, f; Fig. 9c, f).

640

641   Overall, these results help clarify the potential role that the climate-change response of

642   cyclones' core structures have in determining future ET frequency changes, and quantifies

643   how this differs between basins. Differences in pre-ET structures potentially underpin basin-

644   specific responses of ET to climate change, and consistency exists among PRIMAVERA

645   models. However, to fully explain what drives disparate North Atlantic and Western North

646   Pacific responses, further studies of future changes in cyclogenesis and midlatitude large-

647   scale conditions are needed, based on models of higher resolution than those in

648   PRIMAVERA, which better simulate the most intense systems (Judt et al., 2021), and,

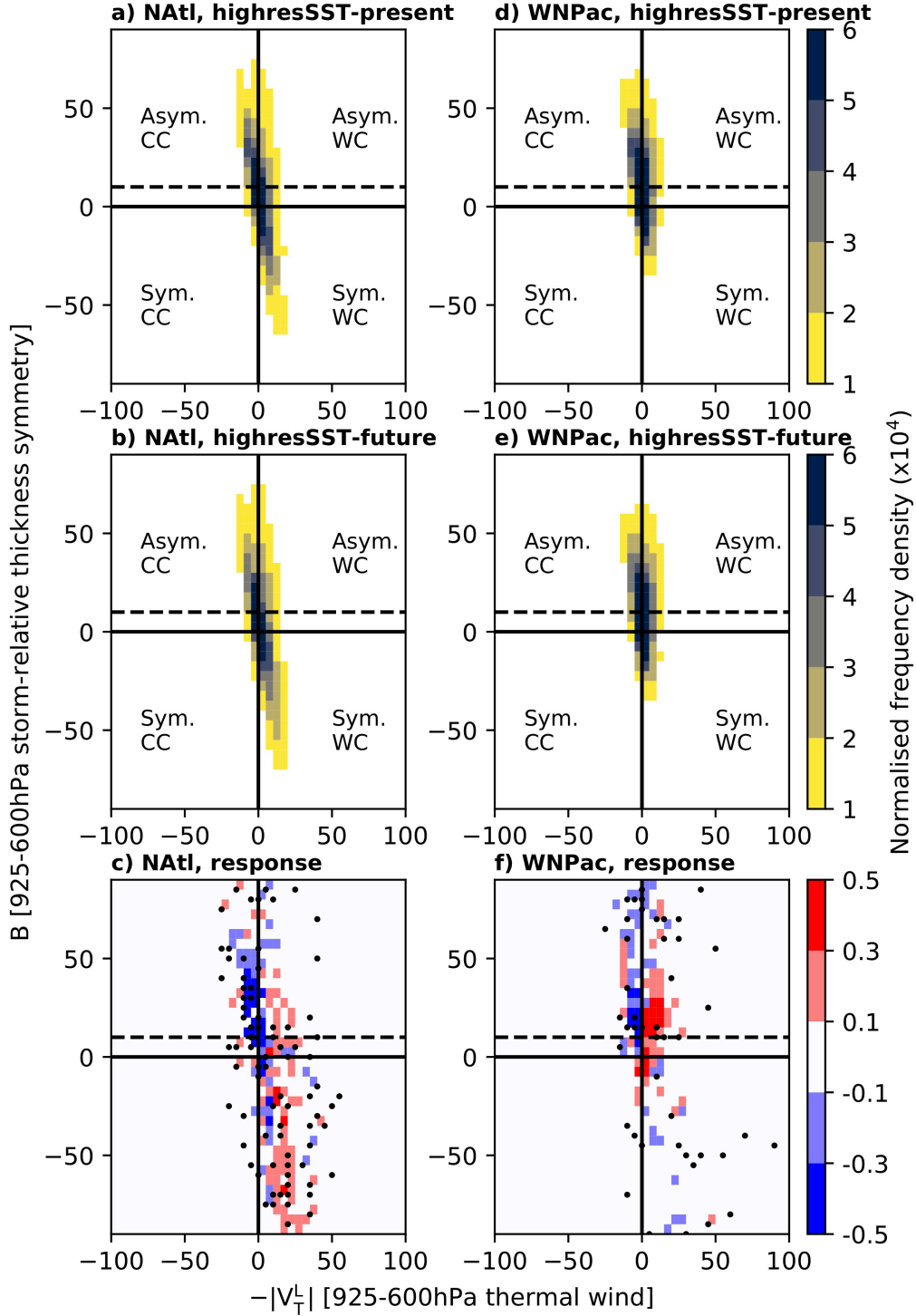649   potentially, their interactions with the large-scale environment.

650

Fig. 6. Ensemble-mean distributions of T_L versus B in high-resolution (a, d) *highresSST-present* and (b, e) *-future* simulations as well as (c, f) the climate-change response for the North Atlantic ('NAtl') and Western North Pacific ('WNPac'). Distributions are computed from every 6-hourly point during the entire lifetime of all storms undergoing ET, plotted as two-dimensional histograms, and normalised by the total number of cyclones (sample sizes for each model are given in Table 3). Values are scaled by 10^4. Cyclone phase-space

658   categories are warm- ('WC') or cold-core ('CC') and either symmetrical (i.e., non-frontal;

659   'Sym.') or asymmetrical (i.e., frontal; 'Asym.'). The threshold of 10 m used to distinguish

660   thermally symmetric from asymmetric cyclones is indicated (dashed line). Stippling in c) and

661   f) indicates where all models agree on the sign of the difference.

662
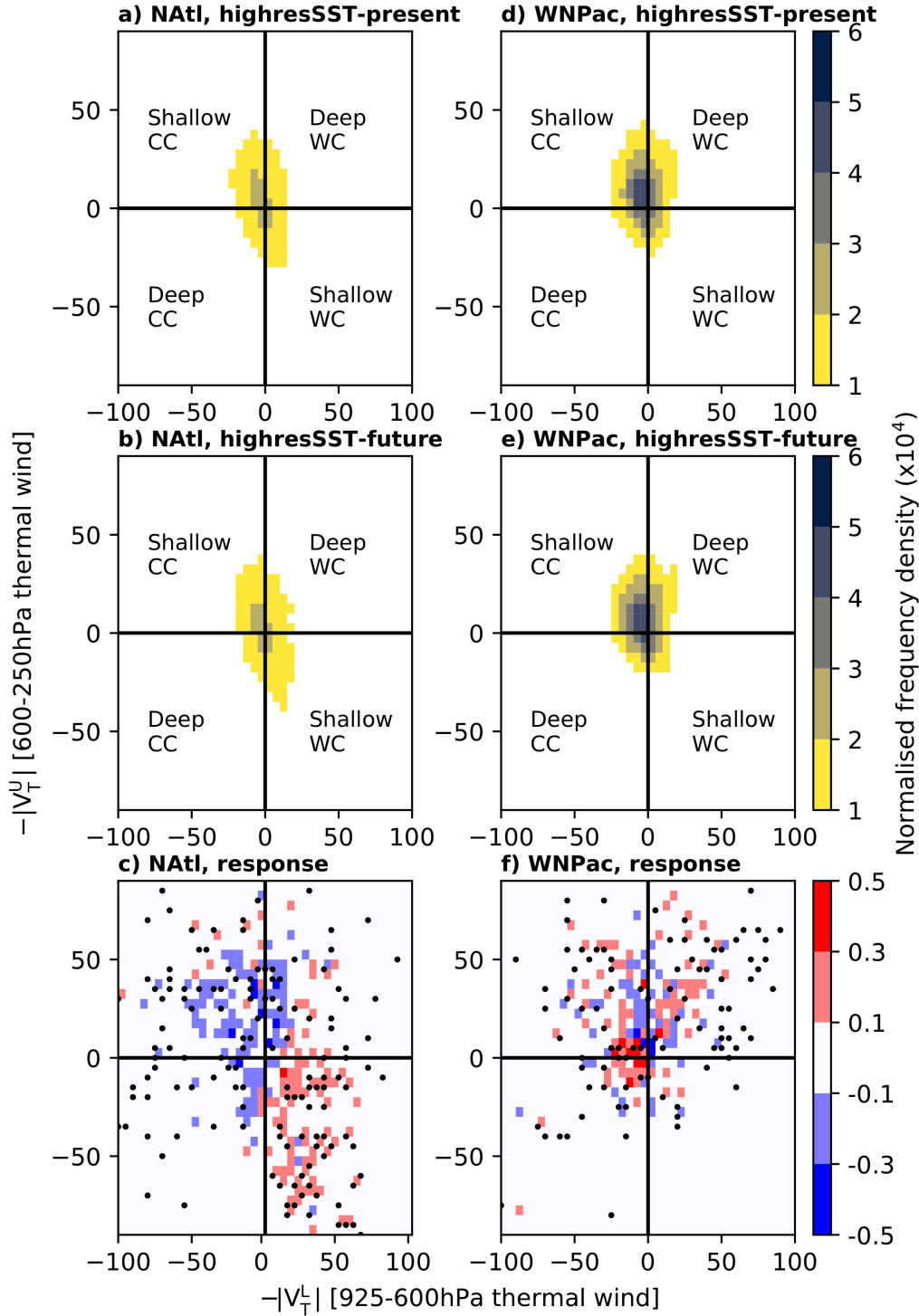
Fig. 7. Ensemble-mean distributions of T_L versus T_U in high-resolution (a, d) *highresSST-present* and (b, e) *-future* simulations as well as (c, f) the climate-change response for the North Atlantic ('NAtl') and Western North Pacific ('WNPac'). Distributions are computed from every 6-hourly point during the entire lifetime of all storms undergoing ET, plotted as two-dimensional histograms, and normalised by the total number of cyclones (sample sizes for each model are given in Table 3). Values are scaled by 10^4. Cyclone phase-space

670   categories are shallow or deep warm- ('WC') or cold-core ('CC'). Stippling in c) and f)

671   indicates where all models agree on the sign of the difference.

672

673
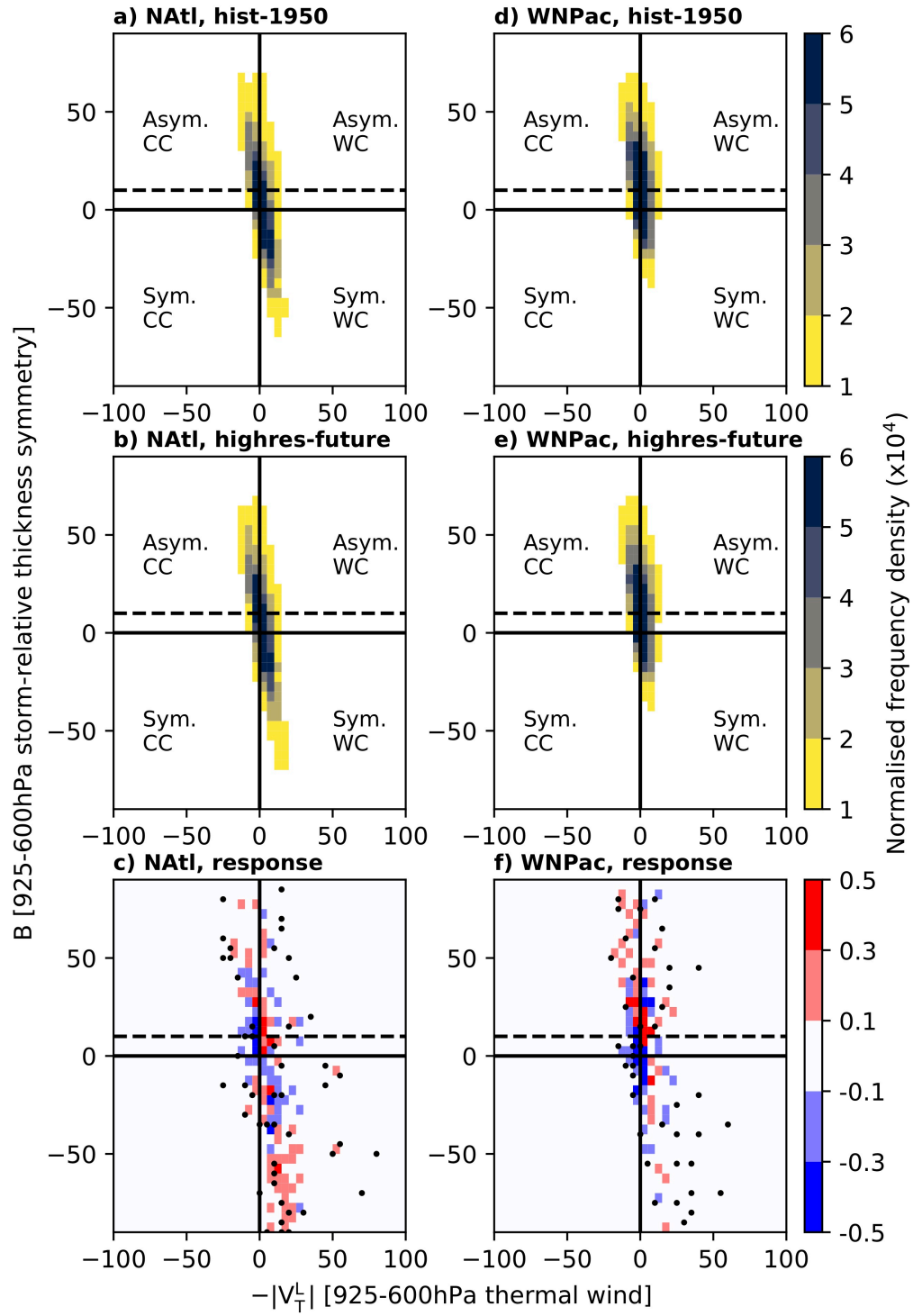
Fig. 8. As in Fig. 6 for *hist-1950* and *highres-future* experiments.
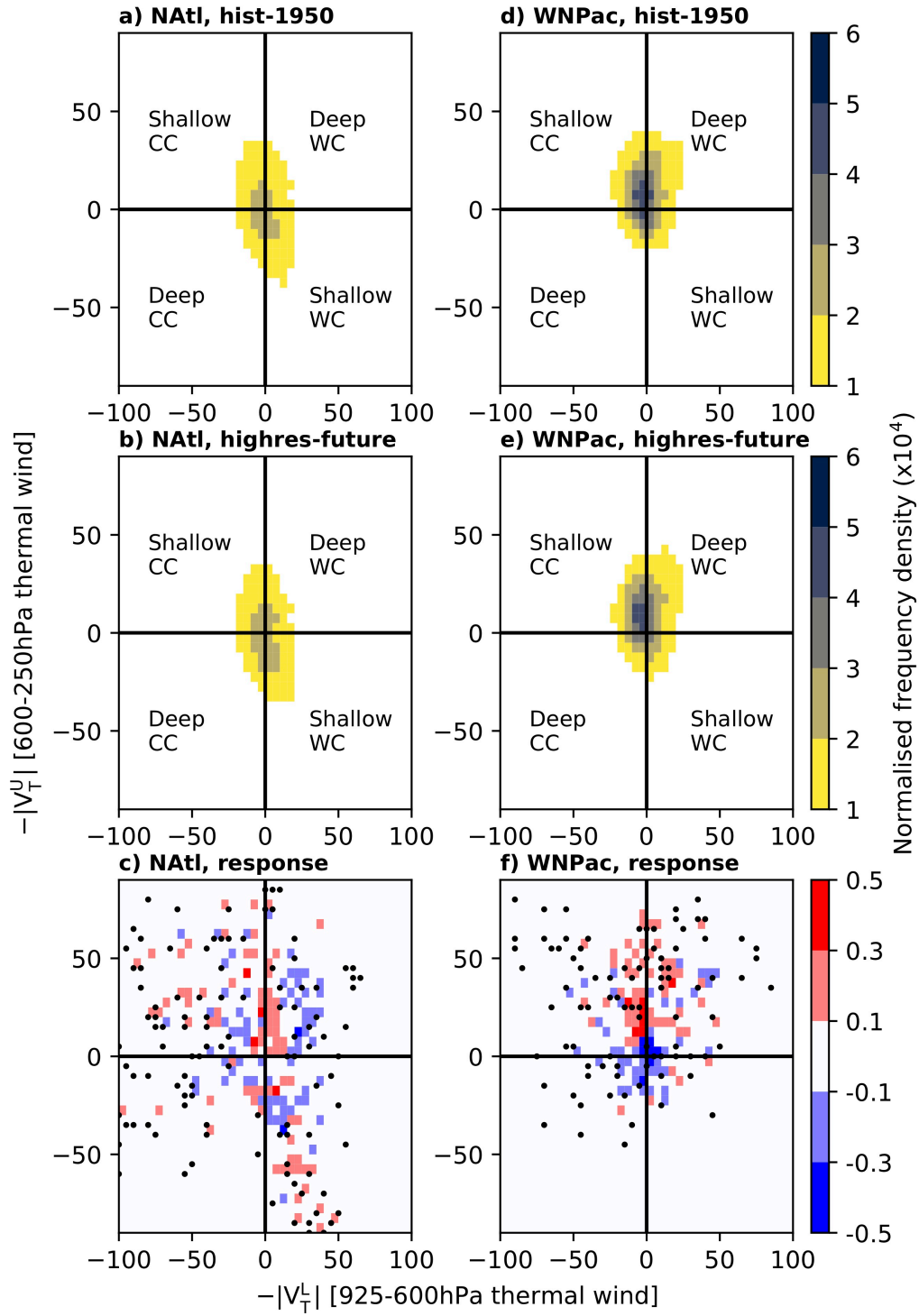
Fig. 9. As in Fig. 7 for *hist-1950* and *highres-future* experiments.

678   *3.5 Pre- and post-ET cyclone intensity*

679   During ET, cyclones develop low-level frontal structures and their horizontal size increases

680   (Evans et al., 2017). As such, increasing model resolution is expected to impact the

681   simulation of cyclones pre- and post-ET differently, particularly in models whose effective

682   resolutions coarsen equatorward. However, performing a global analysis of the pre- and post-

683   ET stages of tropical cyclones' lifecycles is not trivial because ET pathways (i.e., the order in

684   which B and T_L changes occur) differ between ocean basins (Bieli et al., 2019). We therefore

685   separated cyclone tracks' warm- and cold-core stages about ET completion, when both B and

686   T_L satisfy ET criteria, following the definition first used by Hart (2003). Our additional 1-day

687   criterion (see Methods) helps increase confidence in the following inter-model comparison.

688

689   Compared with best-track intensity estimates, certain atmosphere-only models (particularly

690   CNRM-CM6.1) simulate realistic intensities at resolutions in the range 20–50 km (Roberts et

691   al., 2020a). However, best-track intensity estimates are not well suited to evaluating post-ET

692   systems (Velden et al., 2006), and the available primary cyclone wind-speed observations,

693   such as satellite scatterometry data, seldom include cyclones' post-tropical stages and span

694   too short a temporal range for climatological evaluation. We therefore turn to reanalyses,

695   which are constrained by observational data, to provide a homogeneous global reference. An

696   important caveat, however, is the underestimation of cyclone wind speeds in reanalyses

697   (Hodges et al., 2017; Murakami, 2014), although this underestimation is less marked at

698   higher latitudes (Sainsbury et al., 2020).

699

700   Considering all storms globally, PRIMAVERA models reproduce the reanalyses' cold-core,

701   post-ET intensity distributions at both low and high resolution and in both atmosphere-only

702   and fully coupled simulations (Fig. 10 and Fig. 11, top rows). However, models'

703   representation of warm-core, pre-ET distributions improve markedly with increasing

704   resolution, especially for CNRM-CM6.1 and HadGEM3-GC3.1, but more clearly so in the

705   atmosphere-only than in the fully coupled simulations, wherein cold-wake feedbacks reduce

706   upper-ocean temperatures and weaken subsequent tropical cyclones (Balaguru et al., 2014).

707   Sensitivity to resolution is similar in the fully coupled CNRM-CM6.1 and HadGEM3-GC3.1

708   simulations (Fig. 11, top row). These results show that horizontal resolutions typical of

709   CMIP6 appear sufficient to simulate cold-core (post-ET) intensity distributions, including the

710   relatively high-intensity tail—resolutions at which large-ensemble studies to quantify

711   multiannual variability of the strongest post-ET storms are computationally feasible.

712   However, among high-resolution PRIMAVERA models, the high-intensity tail of the warm-

713   core distribution is reproduced only by CNRM-CM6.1.

714

715   For *highresSST-future*, several models project decreasing warm-core and increasing cold-

716   core intensities for weaker storms (<17ms^{-1}) but simulate opposite warm- and cold-core

717   responses for stronger storms (≥17ms^{-1}) (Fig. 10, bottom row). This warm-core response is

718   consistent with projections of intensified tropical cyclones under anthropogenic warming

719   (Knutson et al., 2020). However, these responses are not replicated by fully coupled models

720   (Fig. 11, bottom row), in which intensity changes are weak (Roberts et al., 2020b). In the

721   fully coupled simulations, the responses of pre- and post-ET intensity distributions to climate

722   change are equivocal, with substantial inter-model differences. We speculate that the climate-

723   change forcing out to 2050 in the HighResMIP experimental protocol is insufficiently strong

724   (i.e., the future simulation period is too short) for a clear signal to emerge. However, it is

725   unclear whether intensity changes would be seen. For tropical cyclones overall, Roberts et al.

726   (2020b) found a weak future intensification in these simulations, and Bieli et al. (2020) found

727   equivocal ET climate-change responses in many basins out to 2100 under the weaker RCP4.5

728   scenario. If a clear climate-change signal were to emerge with further increases in model

729   resolution, which would increase the relative difference between the weakest and strongest

730   simulated tropical cyclones, this would suggest that processes important for intensity change
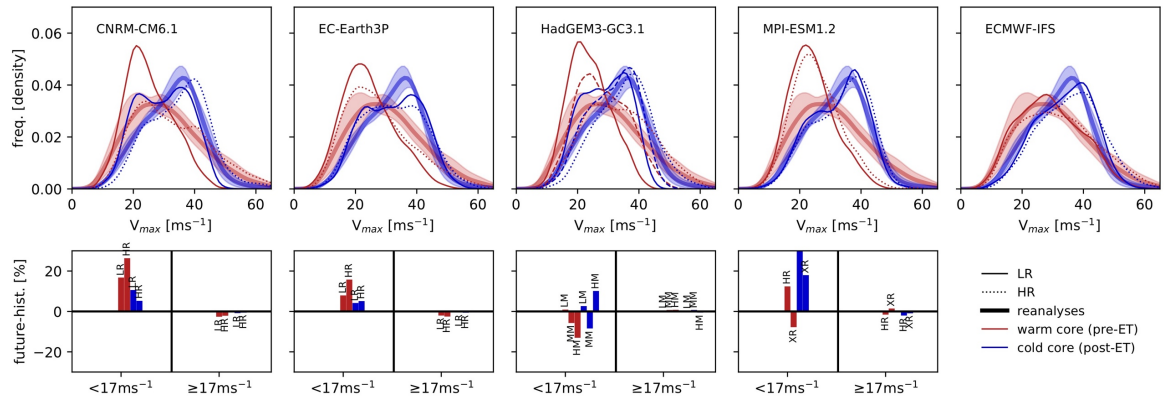
731   are not adequately captured at ~25 km resolution.

732

Fig. 10. Intensity (v_{max} at 925hPa) distributions in atmosphere-only simulations for all cyclones undergoing ET globally. For each model, historical simulations are shown in the top row and future simulations in the bottom row. Multireanalysis-mean curves (thick, solid lines) are shown with 1 s.d. (shading). Both low- (thin, solid lines) and high-resolution (thin, dashed lines) simulations are shown. Climate-change responses (i.e., *highresSST-future* minus *highresSST-present*), computed as integrated differences, are shown as percentages for storms whose lifetime-maximum intensity is <17 ms^{-1} or ≥17 ms^{-1} for each atmospheric model resolution (ordered left to right).
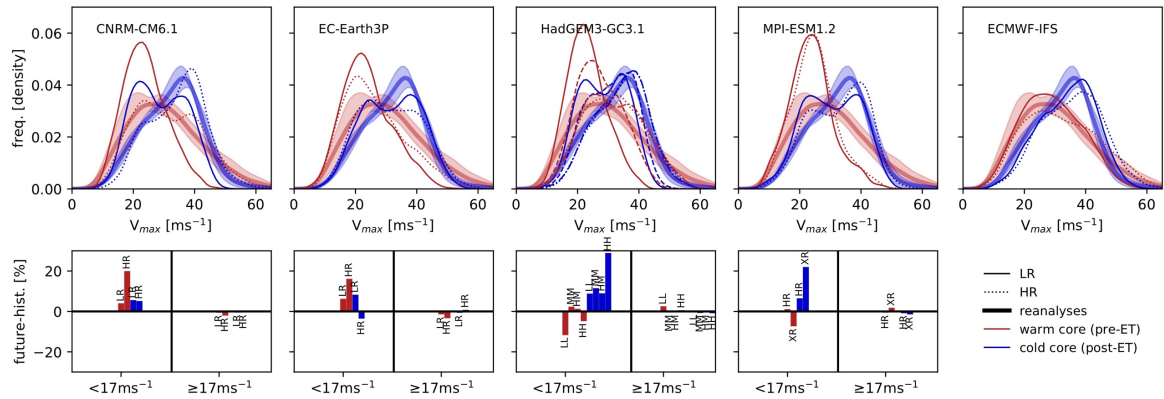
Fig. 11. As in Fig. 10 for fully coupled simulations.

747   *3.6 Post-ET reintensification*

748   The lifetime-maximum intensity of transitioning tropical cyclones typically occurs during the

749   warm-core, tropical phase. However, the addition of a baroclinic energy source and cyclone-

750   wave interactions induce post-ET reintensification (Evans et al., 2017). We quantified the

751   frequencies of reintensifying versus non-reintensifying cyclones in reanalyses and in the

752   PRIMAVERA ensemble. Globally, reanalyses indicate that approximately 50 % of tropical

753   cyclones that complete ET undergo post-ET reintensification (Fig. 12a). For the North

754   Atlantic and Western North Pacific basins, ~55 and ~45 %, respectively, reintensify (not

755   shown), consistent with Hart and Evans (2001). These results are not significantly different

756   when reintensification is defined using 925-hPa wind speed (not shown). Globally,

757   PRIMAVERA models generally overestimate climatological reintensification frequency at

758   low resolution, but increasing resolution decreases the proportion of reintensifying systems

759   (and increases the proportion of non-reintensifying systems) in all models except MPI-

760   ESM1.2, which better matches reanalyses (Fig. 12b and Fig. 13b). This result potentially

761   reflects improved simulation of the interactions between cyclones and the large-scale

762   circulation, which acts to reintensify systems (Keller et al., 2019), at high resolution. Which

763   processes facilitate such improvement should be a focus of future research because these

764   processes will be important for risk assessments of reintensification. However, it is also

765   possible that post-ET reintensification arises in models whose effective resolution increases

766   with increasing latitude (e.g., HadGEM3-GC3.1), allowing stronger simulated winds at

767   higher latitudes, but the impact of this artifact will be reduced at higher resolutions.

768

769   In HadGEM3-GC3.1, for an atmospheric resolution of 25 km (at 50 ° latitude), increasing

770   ocean resolution from 1/4 ° to 1/12 ° (-HM and -HH, respectively) does not impact the

771   proportion of reintensifying cyclones (Fig. 13b). An increase in the proportion might be

772   expected because increasing ocean resolution and therefore more sharply resolving SST

773   fronts (around western boundary currents; Fig. S5) is likely to enhance baroclinicity and

774   provide atmospheric conditions conducive to post-ET reintensification. That no increase is

775   seen implies that atmospheric resolution, to which simulated tropical-cyclone frequency and

776   intensity are sensitive, acts as a constraint on reintensification statistics, at least for this

777   particular model. Further investigation with multiple ocean models would establish more

778   robustly whether this is the case.

779

780   In both the atmosphere-only and fully coupled simulations, future changes in the proportion

781   of post-ET reintensifying systems are small and generally within one standard deviation of

782   historical interannual variability (Fig. 12c and Fig. 13c), again suggesting that any climate-

783   change response under RCP8.5 emerges after 2050. In atmosphere-only simulations, low-

784   resolution models all simulate an increase the proportion of reintensifying cyclones, but high-

785   resolution models simulate a decrease (Fig. 12c), except for CNRM-CM6.1. Fully coupled

786   models typically simulate a future increase across resolutions (Fig. 13c).

787
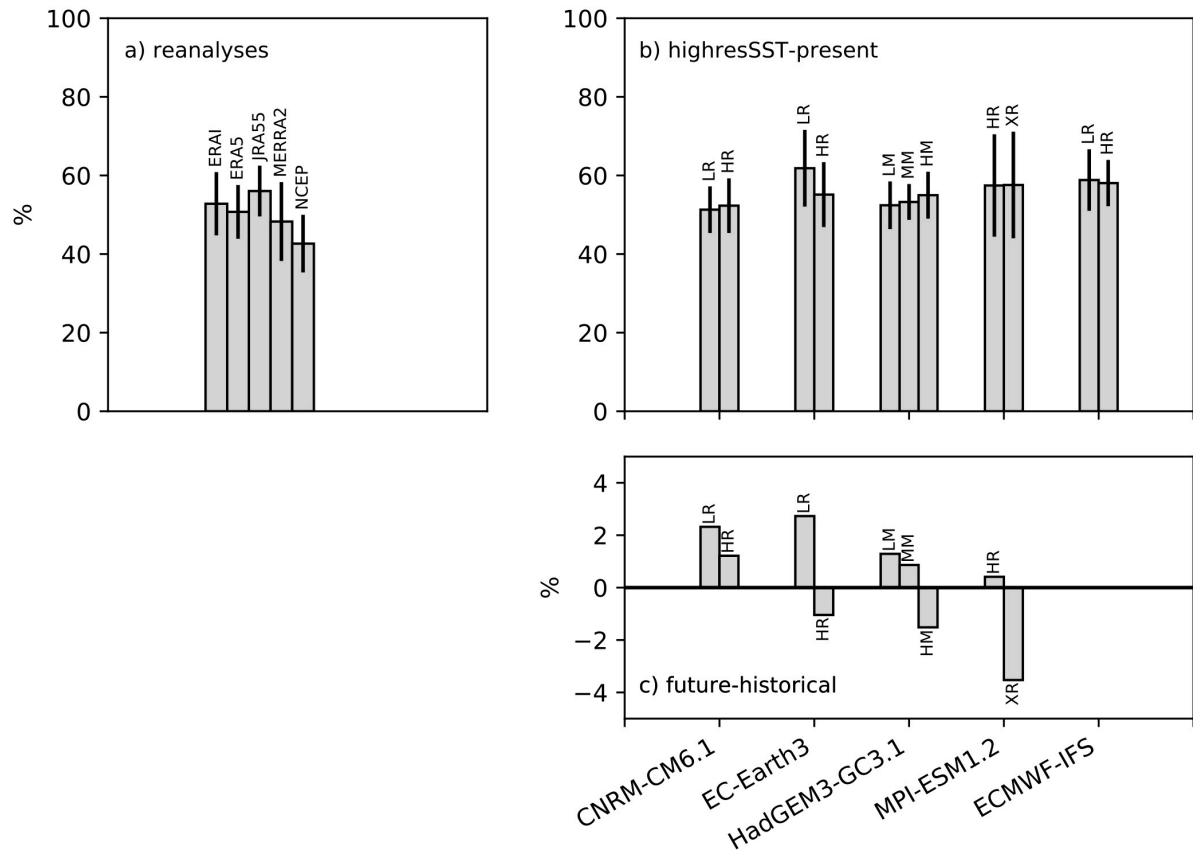
Fig. 12. Global analysis of the percentage of transitioning storms that undergo post-ET reintensification in (a) reanalyses and (b) *highresSST-present* simulations, and (c) the percentage change simulated for *highresSST-future* experiments. One standard deviation of interannual variability is indicated for each reanalysis and historical model simulation (black lines).

795
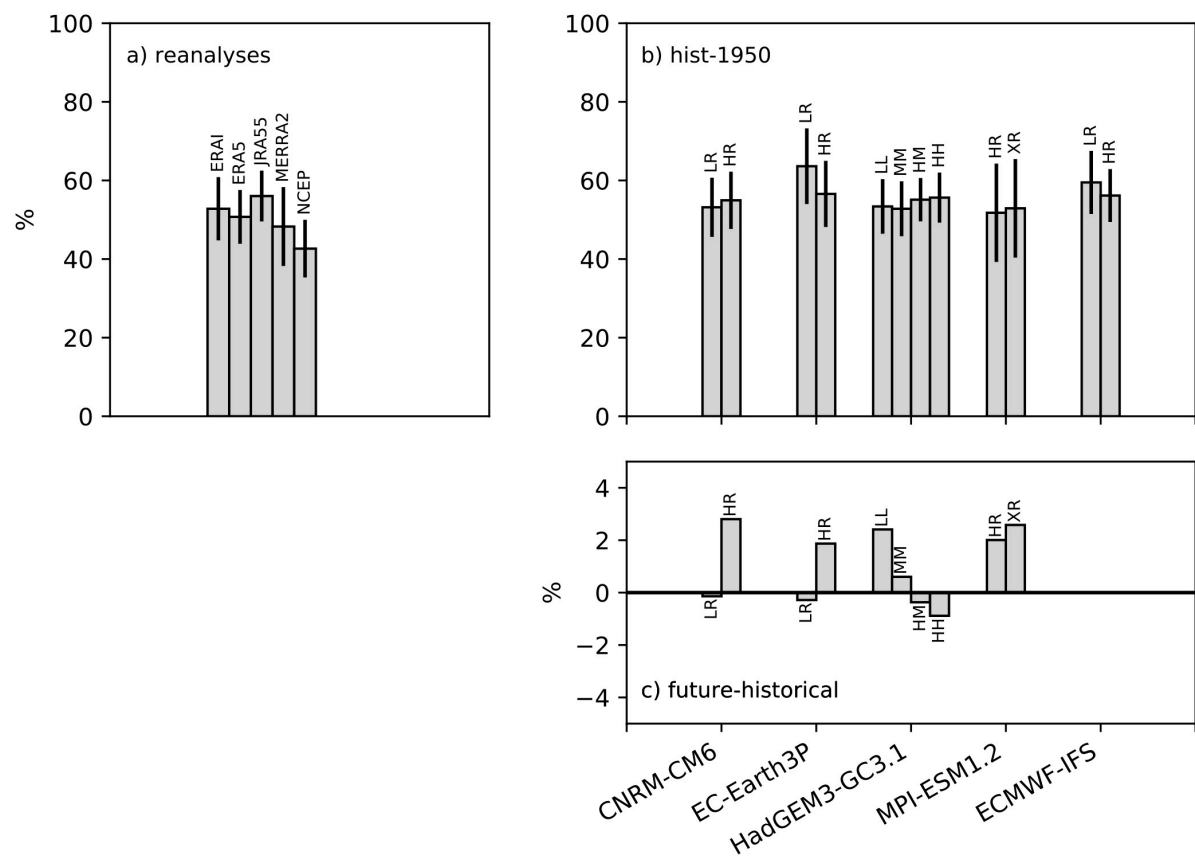
796   **Fig. 13.** As Fig. 12 but for *hist-1950* and *highres-future* simulations.

797

798   *3.7 ET latitude*

799   Finally, we assess how ET location responds to both increased resolution and to climate

800   change out to 2050. Distributions of ET-completion latitude were computed from reanalyses

801   and all PRIMAVERA experiments globally as well as well as separately for the basins where

802   models exhibit the best performance: the North Atlantic and Western North Pacific basins

803   (Fig. 14). For *highresSST-present*, model-simulated ET completion occurs at lower latitudes

804   than in reanalyses (Fig. 14a–c). At high resolution, this is partially rectified: peak frequency

805   occurs at a similar latitude to reanalyses in both the North Atlantic (Fig. 14a) and Western

806   North Pacific (Fig. 14b), but the magnitudes of both peaks are underestimated and

807   occurrences of low-latitude ET (i.e., 10–20 °) remain too frequent. Globally, an equatorward

808   bias in peak frequency across resolutions indicates that ET-completion latitude is less well

809   simulated in other basins (Fig. 14c). These results hold true for *hist-1950* simulations (Fig.

810   14d–f), except there are fewer instances of low-latitude ET (i.e., 10–20 °), likely reflecting

811   slower development of warm-core structures and subsequent ET in the fully coupled

812   experiments.

813

814   In response to climate change, the ensemble-mean distribution of ET-completion latitude

815   exhibits an equatorward shift in the North Atlantic in the atmosphere-only experiment (Fig.

816   14a), but a poleward shift in the fully coupled simulations (Fig. 14d), with an increased

817   frequency of ET completion particularly between 45–55 °N. In the Western North Pacific, a

818   poleward shift is seen in the latitude of the peak frequency, from ~30 to ~40 °N, in both

819   experiments, but little change is simulated at higher latitudes (i.e., > 45 °N). Globally, a small

820   equatorward shift of ~2 ° is simulated in atmosphere-only (Fig. 14c) and no meridional shift

821   is seen in coupled simulations (Fig. 14f). Previously, we showed stronger low-level warm-

822   core structures are simulated in future (Fig. 6 and Fig. 8), which potentially allow tropical

823   cyclones to propagate farther poleward prior to ET, with the most pronounced signal seen in

824   the North Atlantic. While coupled PRIMAVERA models provide evidence for a poleward

825   shift of ET, climate-change responses globally are equivocal out to 2050.
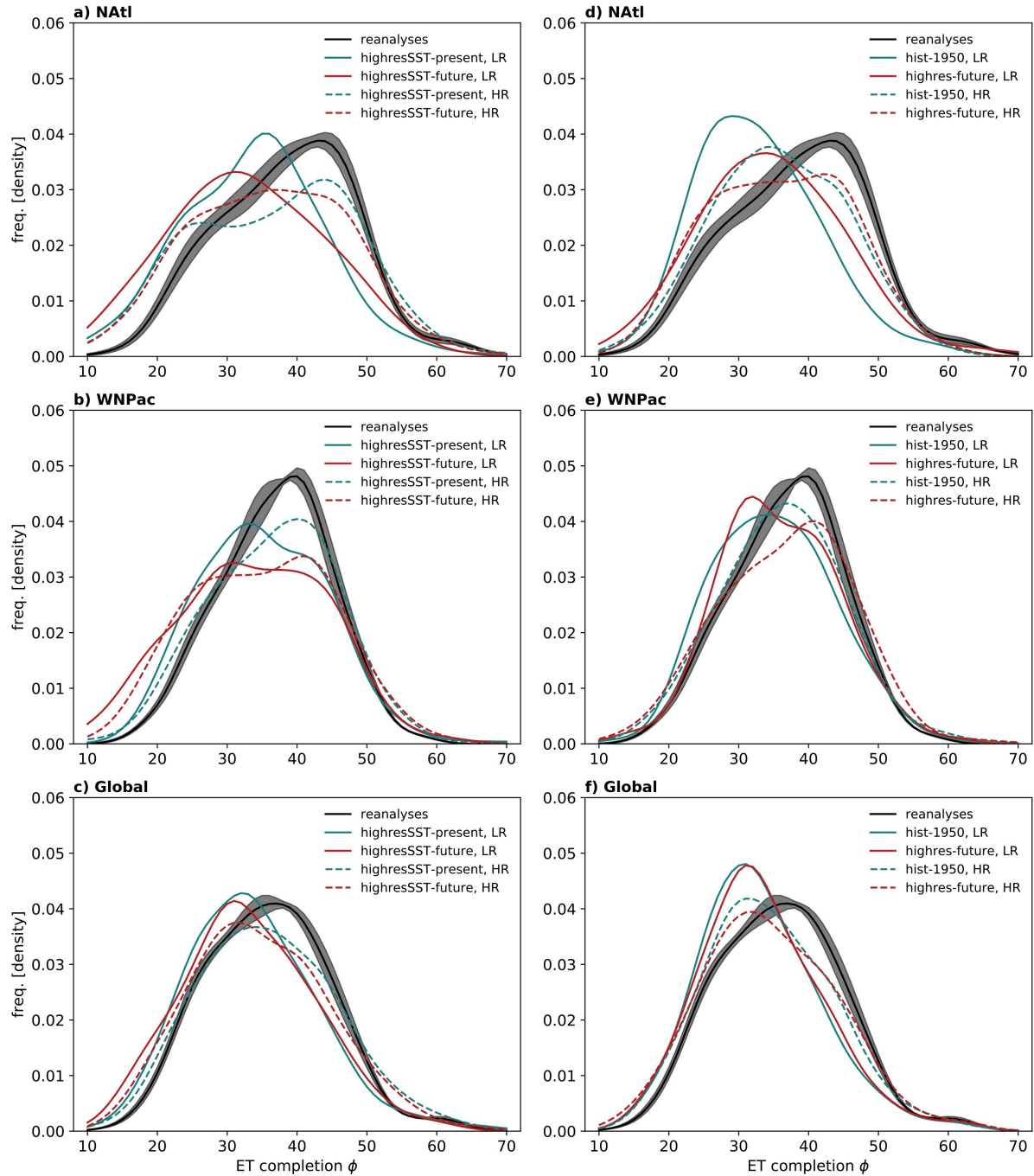
826

827

Fig. 14. Ensemble-mean frequency distributions of ET-completion latitude for (solid lines)
low- and (dashed lines) high-resolution simulations, for both 1950–2014 (teal) and 2015–
2050 (red). Results are shown for (a–c) atmosphere-only and (d–f) fully coupled experiments
for the North Atlantic basin ("NAtl"), Western North Pacific basin ("WNPac") and all global
basins combined. 'LR' and 'HR' denote low- and high-resolution distributions, respectively.
Also shown is the multireanalysis-mean distribution with shading indicating the standard
error for the five reanalyses. Note that frequency is plotted as a function of absolute latitude
(ϕ) to combine Northern and Southern Hemisphere results in c) and f).

836

4. Summary and discussion

This paper presents an analysis of ET across five reanalysis datasets and climate simulations performed with five atmosphere-only and full coupled global models participating in CMIP6 HighResMIP, focussing on (*i*) the effect of increased model resolution on the representation of ET and (*ii*) the response of ET to climate change.

For all tropical cyclones undergoing ET, we find an increase in the climatological track density simulated at high resolution (~25 km) compared with low resolution (~100 km) in all ocean basins and in both atmosphere-only and fully coupled model configurations (Fig. 1b, d), particularly over Northern Hemisphere western boundary currents. Model error in simulated track density (compared with the multireanalysis-mean track density) is reduced at high resolution in the North Atlantic and Western North Pacific (Fig. 1c, e). The simulated climatological annual-mean count of ET events is closer to that of reanalyses in the ocean basins where ET activity is highest—the North Atlantic and the Western and Eastern North Pacific—in both atmosphere-only (Fig. 3) and fully coupled (Fig. 4) experiments. In these basins, atmosphere-only simulations exhibit skill of ~0.3 in capturing interannual variability in just the subset of tropical cyclones that undergo ET (Table 4), demonstrating that the skill of these models in simulating all tropical cyclones does not remain throughout the complete cyclone lifecycle. Additionally, this level of skill in atmosphere-only simulations is lower than that found for similar-resolution initialised seasonal forecasts (Liu et al., 2018). For the other basins—the Northern Indian and Southern Hemisphere—frequencies simulated by high-resolution models overestimate reanalyses. ET %, however, is similar between low- and high-resolution simulations, indicating that the resolution sensitivity of ET is driven by that of tropical cyclone frequency, not by an enhancement of environmental conditions conducive to ET. The seasonal cycle of ET is reproduced by most models, with both the seasonal timing and the magnitude of the seasonal peak simulated more correctly at high-resolution, but the impact of increased atmospheric resolution is model-dependent.

In general, PRIMAVERA models show clearer inter-model agreement on the climate-change response of ET frequency than on the response of intensity-related metrics. For most basins, models simulate a frequency decrease in response to climate change, except over the North Atlantic, where an increase is projected (Fig. 2). The magnitude of the North Atlantic response is larger in atmosphere-only simulations than in fully coupled integrations and is

870   enhanced by increasing atmospheric model resolution, although interannual variability is

871   pronounced (Fig. 3 and Fig. 4). A significant positive trend in the ensemble-mean fraction of

872   North Atlantic ET events occurring during August–November is found over the period 1950–

873   2050 at high-resolution, indicating long-term change in ET seasonality in this basin, but no

874   secular seasonality change is simulated in the Western North Pacific (Fig. 5). North Atlantic

875   seasonality change may result in a higher proportion of tropical cyclones encountering the

876   midlatitude environment during the part of the seasonal cycle when, climatologically,

877   baroclinicity is highest (Hoskins and Hodges, 2019). Opposing future ET responses between

878   the North Atlantic and Western North Pacific are potentially underpinned by changes in low-

879   level, pre-ET warm-core structures, which strengthen in response to climate change in the

880   North Atlantic but undergo little change in the Western North Pacific (Fig. 6 and Fig. 7).

881   Comparing atmosphere-only with fully coupled simulations, the North Atlantic track density

882   response to climate change is more muted in the fully coupled experiment, which is

883   consistent with a less pronounced climate-change response of pre-ET structures simulated by

884   coupled models. Simulations with higher-resolution, storm-resolving models will open

885   opportunities to further study realistically deep warm-core cyclones.

886

887   Globally, simulated warm-core, pre-ET intensity distributions improve with resolution in

888   most models in both atmosphere-only and fully coupled experiments, better resembling

889   reanalyses (Fig. 10 and Fig. 11). Simulated cold-core, post-ET intensity distributions exhibit

890   little sensitivity to resolution across models. Globally, models simulate no clear climate-

891   change response of pre- or post-ET intensity distributions, suggesting that, if a signal exists,

892   extending simulations beyond 2050 may be required. Under *highresSST-future* forcing, some

893   models show decreasing warm-core and increasing cold-core intensities for storms <17ms^{-1},

894   but the opposite response for storms ≥17ms^{-1}. However, this is not reproduced by fully

895   coupled models. Globally, increasing resolution increases the proportion of simulated post-

896   ET reintensifications to approximately match reanalyses, but not in all models. Climate-

897   change responses are not significant with respect to historical interannual variability and are

898   model-dependent (Fig. 12 and Fig. 13).

899

900   The role of model resolution is becoming clearer, but uncertainties remain. Recent analysis of

901   tropical cyclones the PRIMAVERA simulations (Roberts et al., 2020b) has shown that the

902   high-resolution atmosphere-only models, which typically have lower wind-speed biases,

903   show either reduced future wind speeds or no change. Fully coupled models with the smallest

904 historical biases simulate either no change in future wind speeds or increases of only a few

905 percent. These models therefore project weaker intensity responses to climate change

906 compared with other studies (Knutson et al., 2020). One potential factor is the simplifying

907 aspects of the HighResMIP protocol that are necessary to isolate the role of model resolution,

908 particularly the standardised aerosol forcing and use of a single set of SST and sea-ice

909 boundary conditions shared across models (Haarsma et al., 2016). For ET, the climate-change

910 responses of pre- and post-ET intensity analysed in this study are largely model-dependent,

911 with models exhibiting little systematic change between atmospheric resolutions of ~100 and

912 ~25 km. This suggests that these disparate responses are due to differences in model

913 formulation, but a larger ensemble of models is likely needed to assess this fully. For post-ET

914 reintensification, increasing atmospheric resolution appears to result in more consistent

915 model behaviour, but resolution remains a key research issue because several models still

916 underestimate tropical cyclone intensities at ~25 km grid spacing (Roberts et al., 2020a) and

917 further improvements are anticipated by increasing resolution to at least 10 km (Haarsma,

918 2021; Judt et al., 2021). To obtain samples of ET events comparable to this study, however,

919 running sufficiently long simulations (and / or a sufficiently large ensemble) at these storm-

920 resolving resolutions, even without coupling to an ocean model, remains a significant

921 computational challenge (Roberts et al., 2020b).

922

923 Additional outstanding questions and uncertainties remain. A poleward expansion of Hadley

924 circulation termini is projected in a warmer climate (Lu et al., 2007), which implies

925 meridional shifts in tropical storm tracks (Sharmila and Walsh, 2018; Studholme and Gulev,

926 2018). However, the impacts of this large-scale change on the spatial distribution and

927 frequency of ET are equivocal. The poleward expansion of regions conducive to tropical

928 cyclone genesis and development that results from an increase in Hadley cell width will

929 reduce the mean displacement required for tropical cyclones to reach the midlatitude

930 baroclinic zone, increasing the likelihood of ET. However, a poleward shift of the midlatitude

931 storm track in response to warming has been projected (Bengtsson et al., 2006), which in turn

932 shifts environmental conditions conducive to extratropical transition poleward, potentially

933 offsetting Hadley-driven changes. Here, we find minimal changes in ET-completion latitude

934 out to 2050 (Fig. 14), suggesting cancellation in the net effect of these competing large-scale

935 changes. Further work is needed to establish the time of emergence of any meridional shift

936 and will require dedicated studies, exploring a range of climate-change scenarios with models

937   run at resolutions sufficiently high to adequately represent both tropical cyclones and ET—at

938   least 25 km, according to our results.

939

940   This study provides evidence that pre-ET cyclone intensity and warm-core strength exert

941   influence over future changes in ET statistics and seasonality. Analysis of higher-resolution

942   and storm-resolving models (at least 10 km) will help establish whether these results hold

943   true for models able to reproduce more realistic tropical-cyclone maximum intensities,

944   including rapidly intensifying systems. Additionally, there is a need to contextualise future

945   projections of ET, accounting for natural variability, and in particular the roles of regional

946   (e.g., Atlantic Multidecadal Variability) and global (i.e., El Niño–Southern Oscillation)

947   modes of variability on ET frequency. Dedicated sensitivity experiments will be required,

948   and such a study is forthcoming for the North Atlantic, where this work has identified future

949   changes that are important and often unique to this basin. Finally, investigation of secular

950   change in ET seasonality, as seen in the North Atlantic in this study, will be important

951   globally because future modification to the interval between the seasonal maximum of ET

952   occurrence and wintertime storminess may engender considerable changes in risk for

953   populous midlatitude regions.

954

Data and code availability

All reanalysis data for tropical-cyclone tracking (vorticity, wind fields, and sea-level pressure) and cyclone phase-space analysis (geopotential) are available from rda.ucar.edu or disc.gsfc.nasa.gov. Model data are available from Earth System Grid Foundation nodes (esgf.llnl.gov). TRACK is available for download at gitlab.act.reading.ac.uk/track and the track datasets used in this paper may be downloaded from catalogue.ceda.ac.uk/uuid/e82a62d926d7448696a2b60c1925f811. Data analysis and visualisation code is available from the lead author upon request (hrcm.ceda.ac.uk/contact).

Author contributions

AJB, PLV, RJH and MJR conceived the study. Simulations were performed by MJR, ET, KL, CDR, and LT. Output data were managed by JS. MJR performed the cyclone tracking. BV computed Eady growth rate. AJB undertook cyclone phase-space analysis and all other data analyses, figure preparation, and wrote the manuscript. All authors provided input in interpreting results and approved the final manuscript.

Competing interests

The authors declare no competing interests.

985 **References**

986 Arnott, J. M., J. L. Evans, and F. Chiaromonte, 2004: Characterization of Extratropical

987 Transition Using Cluster Analysis. *Monthly Weather Review* **132**, 2916-2937

988 Baatsen, M., R. J. Haarsma, A. J. Van Delden, and H. de Vries, 2015: Severe Autumn storms

989 in future Western Europe with a warmer Atlantic Ocean. *Climate Dynamics* **45**, 949-964

990 Baker, A. J., K. I. Hodges, R. K. H. Schiemann, and P. L. Vidale, 2021: Historical variability

991 and lifecycles of North Atlantic midlatitude cyclones originating in the tropics. *Journal of*

992 *Geophysical Research: Atmospheres* **126**, e2020JD033924

993 Balaguru, K., S. Taraphdar, L. R. Leung, G. R. Foltz, and J. A. Knaff, 2014: Cyclone-cyclone

994 interactions through the ocean pathway. *Geophysical Research Letters* **41**, 6855-6862

995 Barcikowska, M., F. Feser, and H. von Storch, 2012: Usability of Best Track Data in Climate

996 Statistics in the Western North Pacific. *Monthly Weather Review* **140**, 2818-2830

997 Bengtsson, L., K. I. Hodges, and E. Roeckner, 2006: Storm Tracks and Climate Change.

998 *Journal of Climate* **19**, 3518-3543

999 Bieli, M., S. J. Camargo, A. H. Sobel, J. L. Evans, and T. Hall, 2019: A Global Climatology

1000 of Extratropical Transition. Part I: Characteristics across Basins. *Journal of Climate* **32**,

1001 3557-3582

1002 Bieli, M., A. H. Sobel, S. J. Camargo, H. Murakami, and G. A. Vecchi, 2020: Application of

1003 the Cyclone Phase Space to Extratropical Transition in a Global Climate Model. *Journal of*

1004 *Advances in Modeling Earth Systems* **12**, e2019MS001878

1005 Blake, E. S., T. B. Kimberlain, R. J. Berg, C. J.P., and J. L. Beven II, 2013: Hurricane Sandy

1006 (AL182012). *National Hurricane Center Tropical Cyclone Report*,

1007 https://www.nhc.noaa.gov/data/tcr/AL182012_Sandy.pdf

1008 Chang, E. K. M., and Y. Guo, 2007: Is the number of North Atlantic tropical cyclones

1009 significantly underestimated prior to the availability of satellite observations? *Geophysical*

1010 *Research Letters* **34**, L14801

1011   Chu, J.-H., C. R. Sampson, A. S. Levine, and E. Fukada, 2002: The Joint Typhoon Warning

1012   Center Tropical Cyclone Best-Tracks, 1945-2000. United States Naval Research Laboratory,

1013   NRL/MR/7540-02-16.

1014   Davis, C. A., 2018: Resolving Tropical Cyclone Intensity in Models. *Geophysical Research*

1015   *Letters* **45**, 2082-2087

1016   Dee, D. P., S. M. Uppala, A. J. Simmons, P. Berrisford, P. Poli, S. Kobayashi, U. Andrae, M.

1017   A. Balmaseda, G. Balsamo, P. Bauer, P. Bechtold, A. C. M. Beljaars, L. van de Berg, J.

1018   Bidlot, N. Bormann, C. Delsol, R. Dragani, M. Fuentes, A. J. Geer, L. Haimberger, S. B.

1019   Healy, H. Hersbach, E. V. Hólm, L. Isaksen, P. Kållberg, M. Köhler, M. Matricardi, A. P.

1020   McNally, B. M. Monge-Sanz, J. J. Morcrette, B. K. Park, C. Peubey, P. de Rosnay, C.

1021   Tavolato, J. N. Thépaut, and F. Vitart, 2011: The ERA-Interim reanalysis: configuration and

1022   performance of the data assimilation system. *Quarterly Journal of the Royal Meteorological*

1023   *Society* **137**, 553-597

1024   Dekker, M. M., R. J. Haarsma, H. d. Vries, M. Baatsen, and A. J. v. Delden, 2018:

1025   Characteristics and development of European cyclones with tropical origin in reanalysis data.

1026   *Climate Dynamics* **50**, 445-455

1027   Delgado, S., C. W. Landsea, and H. Willoughby, 2018: Reanalysis of the 1954–63 Atlantic

1028   Hurricane Seasons. *Journal of Climate* **31**, 4177-4192

1029   Evans, C., K. M. Wood, S. D. Aberson, H. M. Archambault, S. M. Milrad, L. F. Bosart, K. L.

1030   Corbosiero, C. A. Davis, J. R. D. Pinto, J. Doyle, C. Fogarty, T. J. G. Jr., C. M. Grams, K. S.

1031   Griffin, J. Gyakum, R. E. Hart, N. Kitabatake, H. S. Lentink, R. McTaggart-Cowan, W.

1032   Perrie, J. F. D. Quinting, C. A. Reynolds, M. Riemer, E. A. Ritchie, Y. Sun, and F. Zhang,

1033   2017: The Extratropical Transition of Tropical Cyclones. Part I: Cyclone Evolution and

1034   Direct Impacts. *Monthly Weather Review* **145**, 4317-4344

1035   Grams, C. M., and S. R. Blumer, 2015: European high-impact weather caused by the

1036   downstream response to the extratropical transition of North Atlantic Hurricane Katia (2011).

1037   *Geophysical Research Letters* **42**, 8738-8748

1038   Gutjahr, O., D. Putrasahan, K. Lohmann, J. H. Jungclaus, J. S. von Storch, N. Brüggemann,

1039   H. Haak, and A. Stössel, 2019: Max Planck Institute Earth System Model (MPI-ESM1.2) for

1040   the High-Resolution Model Intercomparison Project (HighResMIP). *Geosci. Model Dev.* **12**,

1041   3241-3281

1042   Haarsma, R., 2021: European Windstorm Risk of Post-Tropical Cyclones and the Impact of

1043   Climate Change. *Geophysical Research Letters* **48**, e2020GL091483

1044   Haarsma, R., M. Acosta, R. Bakhshi, P. A. Bretonnière, L. P. Caron, M. Castrillo, S. Corti, P.

1045   Davini, E. Exarchou, F. Fabiano, U. Fladrich, R. Fuentes Franco, J. García-Serrano, J. von

1046   Hardenberg, T. Koenigk, X. Levine, V. L. Meccia, T. van Noije, G. van den Oord, F. M.

1047   Palmeiro, M. Rodrigo, Y. Ruprich-Robert, P. Le Sager, E. Tourigny, S. Wang, M. van Weele,

1048   and K. Wyser, 2020: HighResMIP versions of EC-Earth: EC-Earth3P and EC-Earth3P-HR –

1049   description, model computational performance and basic validation. *Geosci. Model Dev.* **13**,

1050   3507-3527

1051   Haarsma, R. J., W. Hazeleger, C. Severijns, H. Vries, A. Sterl, R. Bintanja, G. J. Oldenborgh,

1052   and H. W. Brink, 2013: More hurricanes to hit western Europe due to global warming.

1053   *Geophysical Research Letters* **40**, 1783-1788

1054   Haarsma, R. J., M. J. Roberts, P. L. Vidale, C. A. Senior, A. Bellucci, Q. Bao, P. Chang, S.

1055   Corti, N. S. Fučkar, V. Guemas, J. von Hardenberg, W. Hazeleger, C. Kodama, T. Koenigk,

1056   L. R. Leung, J. Lu, J. J. Luo, J. Mao, M. S. Mizielinski, R. Mizuta, P. Nobre, M. Satoh, E.

1057   Scoccimarro, T. Semmler, J. Small, and J. S. von Storch, 2016: High Resolution Model

1058   Intercomparison Project (HighResMIP v1.0) for CMIP6. *Geoscientific Model Development* **9**,

1059   4185-4208

1060   Hagen, A. B., D. Strahan-Sakoskie, and C. Luckett, 2012: A Reanalysis of the 1944–53

1061   Atlantic Hurricane Seasons—The First Decade of Aircraft Reconnaissance. *Journal of*

1062   *Climate* **25**, 4441-4460

1063   Harr, P. A., D. Anwender, and S. C. Jones, 2008: Predictability Associated with the

1064   Downstream Impacts of the Extratropical Transition of Tropical Cyclones: Methodology and

1065   a Case Study of Typhoon Nabi (2005). *Monthly Weather Review* **136**, 3205-3225

1066   Hart, R. E., 2003: A Cyclone Phase Space Derived from Thermal Wind and Thermal

1067   Asymmetry. *Monthly Weather Review* **131**, 585-616

1068   Hart, R. E., and J. L. Evans, 2001: A Climatology of the Extratropical Transition of Atlantic

1069   Tropical Cyclones. *Journal of Climate* **14**, 546-564

1070   Hart, R. E., J. L. Evans, and C. Evans, 2006: Synoptic Composites of the Extratropical

1071   Transition Life Cycle of North Atlantic Tropical Cyclones: Factors Determining

1072   Posttransition Evolution. *Monthly Weather Review* **134**, 553-578

1073   Hersbach, H., B. Bell, P. Berrisford, S. Hirahara, A. Horányi, J. Muñoz-Sabater, J. Nicolas,

1074   C. Peubey, R. Radu, D. Schepers, A. Simmons, C. Soci, S. Abdalla, X. Abellan, G. Balsamo,

1075   P. Bechtold, G. Biavati, J. Bidlot, M. Bonavita, G. De Chiara, P. Dahlgren, D. Dee, M.

1076   Diamantakis, R. Dragani, J. Flemming, R. Forbes, M. Fuentes, A. Geer, L. Haimberger, S.

1077   Healy, R. J. Hogan, E. Hólm, M. Janisková, S. Keeley, P. Laloyaux, P. Lopez, C. Lupu, G.

1078   Radnoti, P. de Rosnay, I. Rozum, F. Vamborg, S. Villaume, and J.-N. Thépaut, 2020: The

1079   ERA5 global reanalysis. *Quarterly Journal of the Royal Meteorological Society* **146**, 1999-

1080   2049

1081   Hodges, K. I., 1995: Feature Tracking on the Unit Sphere. *Monthly Weather Review* **123**,

1082   3458-3465

1083   Hodges, K. I., 1996: Spherical Nonparametric Estimators Applied to the UGAMP Model

1084   Integration for AMIP. *Monthly Weather Review* **124**, 2914-2932

1085   Hodges, K. I., 1999: Adaptive Constraints for Feature Tracking. *Monthly Weather Review*

1086   **127**, 1362-1373

1087   Hodges, K. I., A. Cobb, and P. L. Vidale, 2017: How Well Are Tropical Cyclones

1088   Represented in Reanalysis Datasets? *Journal of Climate* **30**, 5243-5264

1089   Hoskins, B. J., and K. I. Hodges, 2019: The Annual Cycle of Northern Hemisphere Storm

1090   Tracks. Part I: Seasons. *Journal of Climate* **32**, 1743-1760

1091   Hoskins, B. J., and P. J. Valdes, 1990: On the Existence of Storm-Tracks. *Journal of the*

1092   *Atmospheric Sciences* **47**, 1854-1864

1093   Ito, R., T. Takemi, and O. Arakawa, 2016: A Possible Reduction in the Severity of Typhoon

1094   Wind in the Northern Part of Japan under Global Warming: A Case Study. *SOLA* **12**, 100-105

1095 Jones, S. C., P. A. Harr, J. Abraham, L. F. Bosart, P. J. Bowyer, J. L. Evans, D. E. Hanley, B.
1096 N. Hanstrum, R. E. Hart, F. Lalaurette, M. R. Sinclair, R. K. Smith, and C. Thorncroft, 2003:
1097 The Extratropical Transition of Tropical Cyclones: Forecast Challenges, Current
1098 Understanding, and Future Directions. *Weather and Forecasting* **18**, 1052-1092

1099 Judt, F., D. Klocke, R. Rios-Berrios, B. Vannière, F. Ziemen, L. Auger, J. Biercamp, C.
1100 Bretherton, X. Chen, P. Düben, C. Hohenegger, M. Khairoutdinov, C. Kodama, L.
1101 Kornblueh, S.-J. Lin, M. Nakano, P. Neumann, W. Putman, N. Röber, M. Roberts, M. Satoh,
1102 R. Shibuya, B. Stevens, P. L. Vidale, N. Wedi, and L. Zhou, 2021: Tropical Cyclones in
1103 Global Storm-Resolving Models. *Journal of the Meteorological Society of Japan. Ser. II* **99**,
1104 579-602

1105 Jung, C., and G. M. Lackmann, 2021: The Response of Extratropical Transition of Tropical
1106 Cyclones to Climate Change: Quasi-Idealized Numerical Experiments. *Journal of Climate*
1107 **34**, 4361-4381

1108 Keller, J. H., C. M. Grams, M. Riemer, H. M. Archambault, L. Bosart, J. D. Doyle, J. L.
1109 Evans, T. J. G. Jr., K. Griffin, P. A. Harr, N. Kitabatake, R. McTaggart-Cowan, F. Pantillon,
1110 J. F. Quinting, C. A. Reynolds, E. A. Ritchie, R. D. Torn, and F. Zhang, 2019: The
1111 Extratropical Transition of Tropical Cyclones. Part II: Interaction with the Midlatitude Flow,
1112 Downstream Impacts, and Implications for Predictability. *Monthly Weather Review* **147**,
1113 1077-1106

1114 Kitabatake, N., 2011: Climatology of Extratropical Transition of Tropical Cyclones in the
1115 Western North Pacific Defined by Using Cyclone Phase Space. *Journal of the*
1116 *Meteorological Society of Japan. Ser. II* **89**, 309-325

1117 Klaver, R., R. Haarsma, P. L. Vidale, and W. Hazeleger, 2020: Effective resolution in high
1118 resolution global atmospheric models for climate studies. *Atmospheric Science Letters* **21**,
1119 e952

1120 Klein, P. M., P. A. Harr, and R. L. Elsberry, 2002: Extratropical Transition of Western North
1121 Pacific Tropical Cyclones: Midlatitude and Tropical Cyclone Contributions to
1122 Reintensification. *Monthly Weather Review* **130**, 2240-2259

1123 Knutson, T., S. J. Camargo, J. C. L. Chan, K. Emanuel, C.-H. Ho, J. Kossin, M. Mohapatra,

1124 M. Satoh, M. Sugi, K. Walsh, and L. Wu, 2020: Tropical Cyclones and Climate Change

1125 Assessment: Part II: Projected Response to Anthropogenic Warming. *Bulletin of the*

1126 *American Meteorological Society* **101**, E303-E322

1127 Kobayashi, S., Y. Ota, Y. Harada, A. Ebita, M. Moriya, H. Onoda, K. Onogi, H. Kamahori,

1128 C. Kobayashi, H. Endo, K. Miyaoka, and K. Takahashi, 2015: The JRA-55 Reanalysis:

1129 General Specifications and Basic Characteristics. *Journal of the Meteorological Society of*

1130 *Japan. Ser. II* **93**, 5-48

1131 Kofron, D. E., E. A. Ritchie, and J. S. Tyo, 2010: Determination of a Consistent Time for the

1132 Extratropical Transition of Tropical Cyclones. Part I: Examination of Existing Methods for

1133 Finding "ET Time". *Monthly Weather Review* **138**, 4328-4343

1134 Kossin, J. P., K. R. Knapp, D. J. Vimont, R. J. Murnane, and B. A. Harper, 2007: A globally

1135 consistent reanalysis of hurricane variability and trends. *Geophysical Research Letters* **34**

1136 Lanzante, J. R., 2019: Uncertainties in tropical-cyclone translation speed. *Nature* **570**, E6-

1137 E15

1138 Laurila, T. K., V. A. Sinclair, and H. Gregow, 2019: The Extratropical Transition of

1139 Hurricane Debby (1982) and the Subsequent Development of an Intense Windstorm over

1140 Finland. *Monthly Weather Review* **148**, 377-401

1141 Liu, M., G. A. Vecchi, J. A. Smith, and H. Murakami, 2017: The Present-Day Simulation and

1142 Twenty-First-Century Projection of the Climatology of Extratropical Transition in the North

1143 Atlantic. *Journal of Climate* **30**, 2739-2756

1144 Liu, M., G. A. Vecchi, J. A. Smith, H. Murakami, R. Gudgel, and X. Yang, 2018: Towards

1145 Dynamical Seasonal Forecast of Extratropical Transition in the North Atlantic. *Geophysical*

1146 *Research Letters* **45**, 12,602-612,609

1147 Lu, J., G. A. Vecchi, and T. Reichler, 2007: Expansion of the Hadley cell under global

1148 warming. *Geophysical Research Letters* **34**

1149 Manganello, J. V., B. A. Cash, K. I. Hodges, and J. L. Kinter, 2019: Seasonal forecasts of

1150 North Atlantic tropical cyclone activity in the North American Multi-Model Ensemble.

1151 *Climate Dynamics* **53**, 7169-7184

1152 Michaelis, A. C., and G. M. Lackmann, 2019: Climatological Changes in the Extratropical

1153 Transition of Tropical Cyclones in High-Resolution Global Simulations. *Journal of Climate*

1154 **32**, 8733-8753

1155 Michaelis, A. C., and G. M. Lackmann, 2021: Storm-Scale Dynamical Changes of

1156 Extratropical Transition Events in Present-Day and Future High-Resolution Global

1157 Simulations. *Journal of Climate* **34**, 5037-5062

1158 Molod, A., L. Takacs, M. Suarez, and J. Bacmeister, 2015: Development of the GEOS-5

1159 atmospheric general circulation model: evolution from MERRA to MERRA2. *Geosci. Model*

1160 *Dev.* **8**, 1339-1356

1161 Moon, I.-J., S.-H. Kim, and J. C. L. Chan, 2019: Climate change and tropical cyclone trend.

1162 *Nature* **570**, E3-E5

1163 Moreno-Chamarro, E., L. P. Caron, S. Loosveldt Tomas, J. Vegas-Regidor, O. Gutjahr, M. P.

1164 Moine, D. Putrasahan, C. D. Roberts, M. J. Roberts, R. Senan, L. Terray, E. Tourigny, and P.

1165 L. Vidale, 2022: Impact of increased resolution on long-standing biases in HighResMIP-

1166 PRIMAVERA climate models. *Geosci. Model Dev.* **15**, 269-289

1167 Murakami, H., 2014: Tropical cyclones in reanalysis data sets. *Geophysical Research Letters*

1168 **41**, 2133-2141

1169 Rantanen, M., J. Räisänen, V. A. Sinclair, J. Lento, and H. Järvinen, 2020: The extratropical

1170 transition of Hurricane Ophelia (2017) as diagnosed with a generalized omega equation and

1171 vorticity equation. *Tellus A: Dynamic Meteorology and Oceanography* **72**, 1-26

1172 Roberts, C. D., R. Senan, F. Molteni, S. Boussetta, M. Mayer, and S. P. E. Keeley, 2018:

1173 Climate model configurations of the ECMWF Integrated Forecasting System (ECMWF-IFS

1174 cycle 43r1) for HighResMIP. *Geosci. Model Dev.* **11**, 3681-3712

1175 Roberts, M. J., A. Baker, E. W. Blockley, D. Calvert, A. Coward, H. T. Hewitt, L. C.

1176 Jackson, T. Kuhlbrodt, P. Mathiot, C. D. Roberts, R. Schiemann, J. Seddon, B. Vannière, and

1177   P. L. Vidale, 2019: Description of the resolution hierarchy of the global coupled HadGEM3-

1178   GC3.1 model as used in CMIP6 HighResMIP experiments. *Geosci. Model Dev.* **12**, 4999-

1179   5028

1180   Roberts, M. J., J. Camp, J. Seddon, P. L. Vidale, K. Hodges, B. Vanniere, J. Mecking, R.

1181   Haarsma, A. Bellucci, E. Scoccimarro, L.-P. Caron, F. Chauvin, L. Terray, S. Valcke, M.-P.

1182   Moine, D. Putrasahan, C. Roberts, R. Senan, C. Zarzycki, and P. Ullrich, 2020a: Impact of

1183   Model Resolution on Tropical Cyclone Simulation Using the HighResMIP–PRIMAVERA

1184   Multimodel Ensemble. *Journal of Climate* **33**, 2557-2583

1185   Roberts, M. J., J. Camp, J. Seddon, P. L. Vidale, K. Hodges, B. Vannière, J. Mecking, R.

1186   Haarsma, A. Bellucci, E. Scoccimarro, L.-P. Caron, F. Chauvin, L. Terray, S. Valcke, M.-P.

1187   Moine, D. Putrasahan, C. D. Roberts, R. Senan, C. Zarzycki, P. Ullrich, Y. Yamada, R.

1188   Mizuta, C. Kodama, D. Fu, Q. Zhang, G. Danabasoglu, N. Rosenbloom, H. Wang, and L.

1189   Wu, 2020b: Projected Future Changes in Tropical Cyclones Using the CMIP6 HighResMIP

1190   Multimodel Ensemble. *Geophysical Research Letters* **47**, e2020GL088662

1191   Roberts, M. J., P. L. Vidale, M. S. Mizielinski, M.-E. Demory, R. Schiemann, J. Strachan, K.

1192   Hodges, R. Bell, and J. Camp, 2015: Tropical Cyclones in the UPSCALE Ensemble of High-

1193   Resolution Global Climate Models. *Journal of Climate* **28**, 574-596

1194   Saha, S., S. Moorthi, X. Wu, J. Wang, S. Nadiga, P. Tripp, D. Behringer, Y.-T. Hou, H.-y.

1195   Chuang, M. Iredell, M. Ek, J. Meng, R. Yang, M. P. Mendez, H. v. d. Dool, Q. Zhang, W.

1196   Wang, M. Chen, and E. Becker, 2014: The NCEP Climate Forecast System Version 2.

1197   *Journal of Climate* **27**, 2185-2208

1198   Sainsbury, E. M., R. K. H. Schiemann, K. I. Hodges, L. C. Shaffrey, A. J. Baker, and K. T.

1199   Bhatia, 2020: How Important Are Post-Tropical Cyclones for European Windstorm Risk?

1200   *Geophysical Research Letters* **47**, e2020GL089853

1201   Schreck III, C. J., K. R. Knapp, and J. P. Kossin, 2014: The Impact of Best Track

1202   Discrepancies on Global Tropical Cyclone Climatologies using IBTrACS. *Monthly Weather*

1203   *Review* **142**, 3881-3899

1204   Sharmila, S., and K. J. E. Walsh, 2018: Recent poleward shift of tropical cyclone formation

1205   linked to Hadley cell expansion. *Nature Climate Change* **8**, 730-736

1206   Stewart, S. R., 2018: Hurricane Ophelia (AL172017). *National Hurricane Center Tropical*

1207   *Cyclone Report*, www.nhc.noaa.gov/data/tcr/AL172017_Ophelia.pdf

1208   Strachan, J., P. L. Vidale, K. Hodges, M. Roberts, and M.-E. Demory, 2013: Investigating

1209   Global Tropical Cyclone Activity with a Hierarchy of AGCMs: The Role of Model

1210   Resolution. *Journal of Climate* **26**, 133-152

1211   Studholme, J., A. V. Fedorov, S. K. Gulev, K. Emanuel, and K. Hodges, 2022: Poleward

1212   expansion of tropical cyclone latitudes in warming climates. *Nature Geoscience* **15**, 14-28

1213   Studholme, J., and S. Gulev, 2018: Concurrent Changes to Hadley Circulation and the

1214   Meridional Distribution of Tropical Cyclones. *Journal of Climate* **31**, 4367-4389

1215   Studholme, J., K. I. Hodges, and C. M. Brierley, 2015: Objective determination of the

1216   extratropical transition of tropical cyclones in the Northern Hemisphere. *Tellus A: Dynamic*

1217   *Meteorology and Oceanography* **67**, 24474

1218   Vannière, B., M. Roberts, P. L. Vidale, K. Hodges, M.-E. Demory, L.-P. Caron, E.

1219   Scoccimarro, L. Terray, and R. Senan, 2020: The Moisture Budget of Tropical Cyclones in

1220   HighResMIP Models: Large-Scale Environmental Balance and Sensitivity to Horizontal

1221   Resolution. *Journal of Climate* **33**, 8457-8474

1222   Vecchi, G. A., T. L. Delworth, H. Murakami, S. D. Underwood, A. T. Wittenberg, F. Zeng,

1223   W. Zhang, J. W. Baldwin, K. T. Bhatia, W. Cooke, J. He, S. B. Kapnick, T. R. Knutson, G.

1224   Villarini, K. van der Wiel, W. Anderson, V. Balaji, J. H. Chen, K. W. Dixon, R. Gudgel, L.

1225   M. Harris, L. Jia, N. C. Johnson, S.-J. Lin, M. Liu, C. H. J. Ng, A. Rosati, J. A. Smith, and X.

1226   Yang, 2019: Tropical cyclone sensitivities to CO2 doubling: roles of atmospheric resolution,

1227   synoptic variability and background climate changes. *Climate Dynamics* **53**, 5999-6033

1228   Vecchi, G. A., and T. R. Knutson, 2008: On Estimates of Historical North Atlantic Tropical

1229   Cyclone Activity. *Journal of Climate* **21**, 3580-3600

1230   Vecchi, G. A., and T. R. Knutson, 2011: Estimating Annual Numbers of Atlantic Hurricanes

1231   Missing from the HURDAT Database (1878–1965) Using Ship Track Density. *Journal of*

1232   *Climate* **24**, 1736-1746

1233 Velden, C., B. Harper, F. Wells, J. L. Beven, R. Zehr, T. Olander, M. Mayfield, C. C. Guard,

1234 M. Lander, R. Edson, L. Avila, A. Burton, M. Turk, A. Kikuchi, A. Christian, P. Caroff, and

1235 P. McCrone, 2006: The Dvorak Tropical Cyclone Intensity Estimation Technique: A

1236 Satellite-Based Method that Has Endured for over 30 Years. *Bulletin of the American*

1237 *Meteorological Society* **87**, 1195-1210

1238 Vidale, P. L., K. Hodges, B. Vannière, P. Davini, M. J. Roberts, K. Strommen, A.

1239 Weisheimer, E. Plesca, and S. Corti, 2021: Impact of Stochastic Physics and Model

1240 Resolution on the Simulation of Tropical Cyclones in Climate GCMs. *Journal of Climate* **34**,

1241 4315-4341

1242 Voldoire, A., D. Saint-Martin, S. Sénési, B. Decharme, A. Alias, M. Chevallier, J. Colin, J. F.

1243 Guérémy, M. Michou, M. P. Moine, P. Nabat, R. Roehrig, D. Salas y Mélia, R. Séférian, S.

1244 Valcke, I. Beau, S. Belamari, S. Berthet, C. Cassou, J. Cattiaux, J. Deshayes, H. Douville, C.

1245 Ethé, L. Franchistéguy, O. Geoffroy, C. Lévy, G. Madec, Y. Meurdesoif, R. Msadek, A.

1246 Ribes, E. Sanchez-Gomez, L. Terray, and R. Waldman, 2019: Evaluation of CMIP6 DECK

1247 Experiments With CNRM-CM6-1. *Journal of Advances in Modeling Earth Systems* **11**, 2177-

1248 2213

1249 Weinkle, J., C. Landsea, D. Collins, R. Musulin, R. P. Crompton, P. J. Klotzbach, and R.

1250 Pielke, 2018: Normalized hurricane damage in the continental United States 1900–2017.

1251 *Nature Sustainability* **1**, 808-813

1252 Williams, K. D., D. Copsey, E. W. Blockley, A. Bodas-Salcedo, D. Calvert, R. Comer, P.

1253 Davis, T. Graham, H. T. Hewitt, R. Hill, P. Hyder, S. Ineson, T. C. Johns, A. B. Keen, R. W.

1254 Lee, A. Megann, S. F. Milton, J. G. L. Rae, M. J. Roberts, A. A. Scaife, R. Schiemann, D.

1255 Storkey, L. Thorpe, I. G. Watterson, D. N. Walters, A. West, R. A. Wood, T. Woollings, and

1256 P. K. Xavier, 2018: The Met Office Global Coupled Model 3.0 and 3.1 (GC3.0 and GC3.1)

1257 Configurations. *Journal of Advances in Modeling Earth Systems* **10**, 357-380

1258 Wood, K. M., and E. A. Ritchie, 2014: A 40-Year Climatology of Extratropical Transition in

1259 the Eastern North Pacific. *Journal of Climate* **27**, 5999-6015

1260 Zarzycki, C. M., D. R. Thatcher, and C. Jablonowski, 2017: Objective tropical cyclone

1261 extratropical transition detection in high-resolution reanalysis and climate model data.

1262 *Journal of Advances in Modeling Earth Systems* **9**, 130-148

1263   Zhu, X., L. Wu, and Q. Wang, 2018: Extratropical Transition and Re-Intensification of

1264   Typhoon Toraji (2001): Large-Scale Circulations, Structural Characteristics, and Mechanism

1265   Analysis. *Journal of Ocean University of China* **17**, 461-476

1266

Supplementary information

Extratropical transition of tropical cyclones in a multiresolution ensemble of atmosphere-only and fully coupled global climate models

Alexander J. Baker[1,*], Malcolm J. Roberts[2], Pier Luigi Vidale[1], Kevin I. Hodges[1], Jon Seddon[2], Benoît Vannière[1], Rein J. Haarsma[3], Reinhard Schiemann[1], Dimitris Kapetanakis[3], Etienne Tourigny[4], Katja Lohmann[5], Christopher D. Roberts[6], and Laurent Terray[7]

[1] National Centre for Atmospheric Science and Department of Meteorology, University of Reading, Reading, Berkshire, UK
[2] Met Office Hadley Centre, Exeter, Devon, UK
[3] Koninklijk Nederlands Meteorologisch Instituut, De Bilt, The Netherlands
[4] Earth Sciences Department, Barcelona Supercomputing Center, Barcelona, Spain
[5] Max Planck Institut für Meteorologie, Hamburg, Germany
[6] European Centre for Medium-Range Weather Forecasts (ECMWF), Reading, UK
[7] Climat, Environnement, Couplages et Incertitudes, Centre Européen de Recherche et de Formation Avancée en Calcul Scientifique (CERFACS), Toulouse, France
* alexander.baker@reading.ac.uk

Corresponding author: Dr Alexander J. Baker

National Centre for Atmospheric Science
Department of Meteorology,
University of Reading
Earley Gate, Whiteknights Road, Reading, Berkshire RG6 6ES, UK
+44 (0) 118 377 762

S1. Methodological considerations

Two important methodological considerations in ET studies are discussed in this section: (*i*) the cyclone-tracking algorithm and (*ii*) the sensitivity of ET location to how ET is identified.

S1.1 Cyclone-tracking algorithm

Recent studies of tropical cyclones in reanalyses and simulated by climate models (e.g., Roberts et al., 2020a; Vannière et al., 2020) compared results obtained using TRACK with TempestExtremes, a sea-level-pressure-based tracking algorithm (Ullrich and Zarzycki, 2017), to show that, broadly, their results are robust to algorithm choice. However, tracks output by TempestExtremes represent only cyclones' warm-core stages, and as such few identified systems undergo ET (Fig. S1). Therefore, supplementary algorithms are required to extend cyclone tracks generated using TempestExtremes into the midlatitudes (e.g., Michaelis and Lackmann, 2019; Zarzycki et al., 2017), but the extent to which results are sensitive to the additional methodological choices necessary in this approach is unclear. In this study, use of TRACK, a vorticity-based algorithm that satisfactorily yields complete cyclone lifecycles based on a single set of identification criteria, is clearly advantageous in our analysis of ET statistics. Once comparable whole-lifecycle tracks, including post-tropical evolution, from multiple, independent algorithms are available, sensitivity analysis should be a research priority.
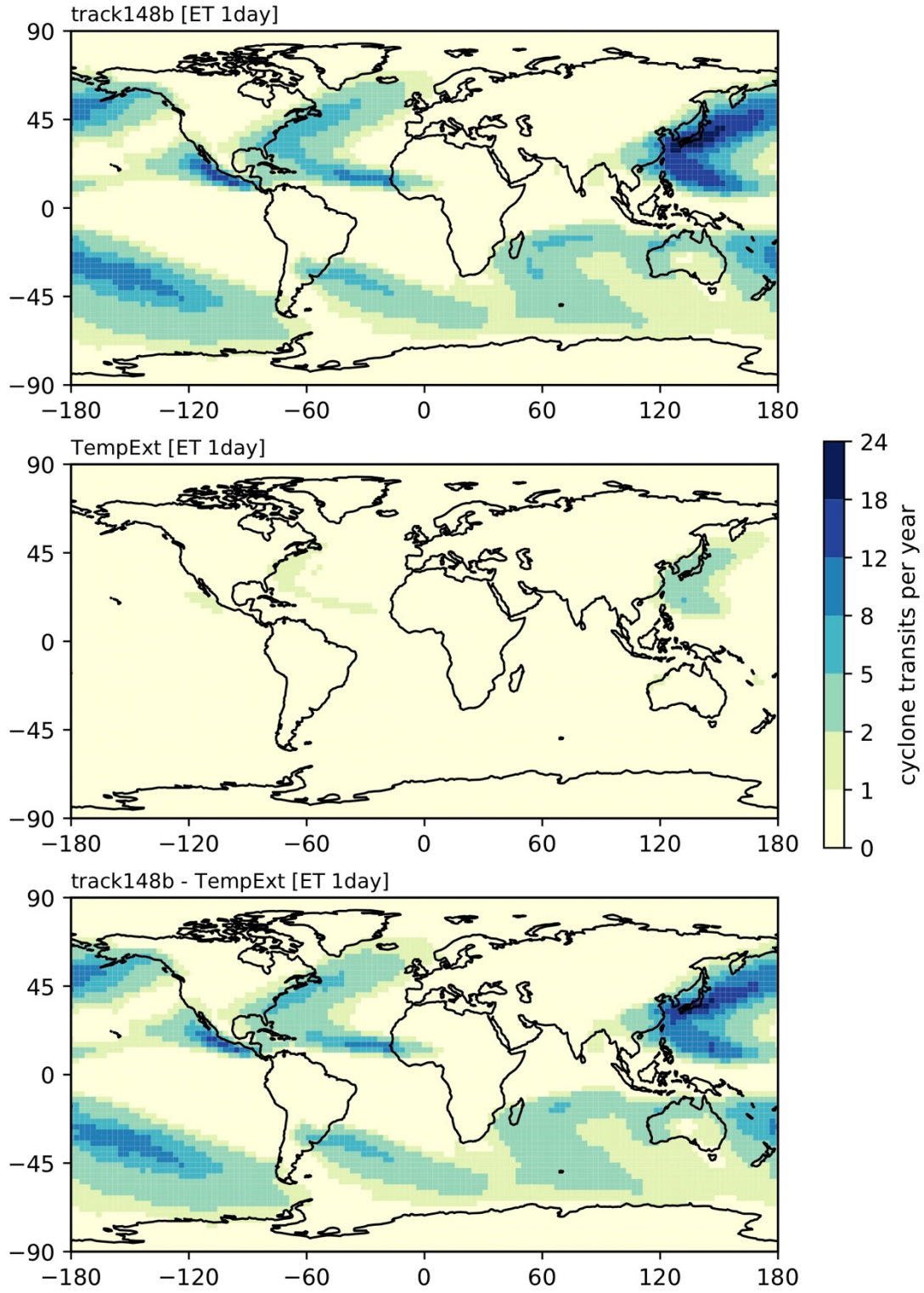
Fig. S1. Multi-reanalysis-mean track density in TCs undergoing ET identified by two feature-tracking algorithms: (top) TRACK ('track148b") and (middle) TempestExtremes ("TempExt"). We also show (bottom) the inter-algorithm difference (i.e., TRACK minus TempestExtremes).

S1.2 Sensitivity of ET location to identification method

Recent analysis of ERA5 shows that phase-space-based identification of post-tropical structures compares well with other methods in terms of the number of ET events identified (Sainsbury et al., 2020) and phase-space methodologies are the most common across studies of ET. However, no consensus approach to identifying ET onset and completion based on phase-space parameters exists. Previous studies have applied differing absolute thresholds to identify changes in cyclone thermal symmetry and employed additional criteria, such as intensity thresholds and temporal smoothing of phase-space series. These modifications have little impact on the number of identified events, but the location of ET may be sensitive to how phase-space parameters are treated. We conducted an overview assessment of this in reanalyses by mapping the mean ET-completion locations for various identification approaches (Fig. S2). In the North Atlantic and Western North Pacific, a definition of ET where both ET onset and completion are identified by single-timestep B or T_L changes ('conventional') yields the lowest-latitude ET completion (Fig. S2). In contrast, applying a prior warm-core test, as in the previous section (4.2), yields ET completion in the range of 30–40 ° latitude, coinciding with the known centres of baroclinicity associated with western boundary currents. Other proposed modifications of ET identification—imposing a v_{max} threshold, applying a temporal smoothing, and requiring B and T_L criteria are met for consecutive timesteps—yield locations in between these two approaches, with greater overlap seen in the Western North Pacific (Fig. S2). These results help quantify the sensitivity of ET location to various methodological choices, and the results presented in Fig. 16 are necessarily sensitive to such choices, as are other published analyses. The method should fit the research question. When ET completion is identified post-warm core, it is broadly co-located with climatological, basin-high values of Eady growth rate (Fig. S2), indicating that this approach may be preferable for analyses of ET location, particularly in the North Atlantic.

In addition, application to climate models presents additional concerns. Bieli et al. (2020) identified grid-scale convective updrafts in 50-km-resolution simulations with the Forecast-oriented Low Ocean Resolution (FLOR) version of the GFDL CM2.5 that triggered erroneous diagnoses of warm- and cold-core cyclone structures. These were rectified by computing storm-centric 95th-percentile geopotential (rather than local maxima) and by applying a temporal smoothing to phase-space trajectories. Although these issues are not pertinent to all models, understanding the effect of convection-parameterisation schemes on geopotential maxima and phase-space results, particularly T_U, requires a systematic investigation across

multiple high-resolution models, contrasting simulations run using parameterised versus explicitly resolved convection.
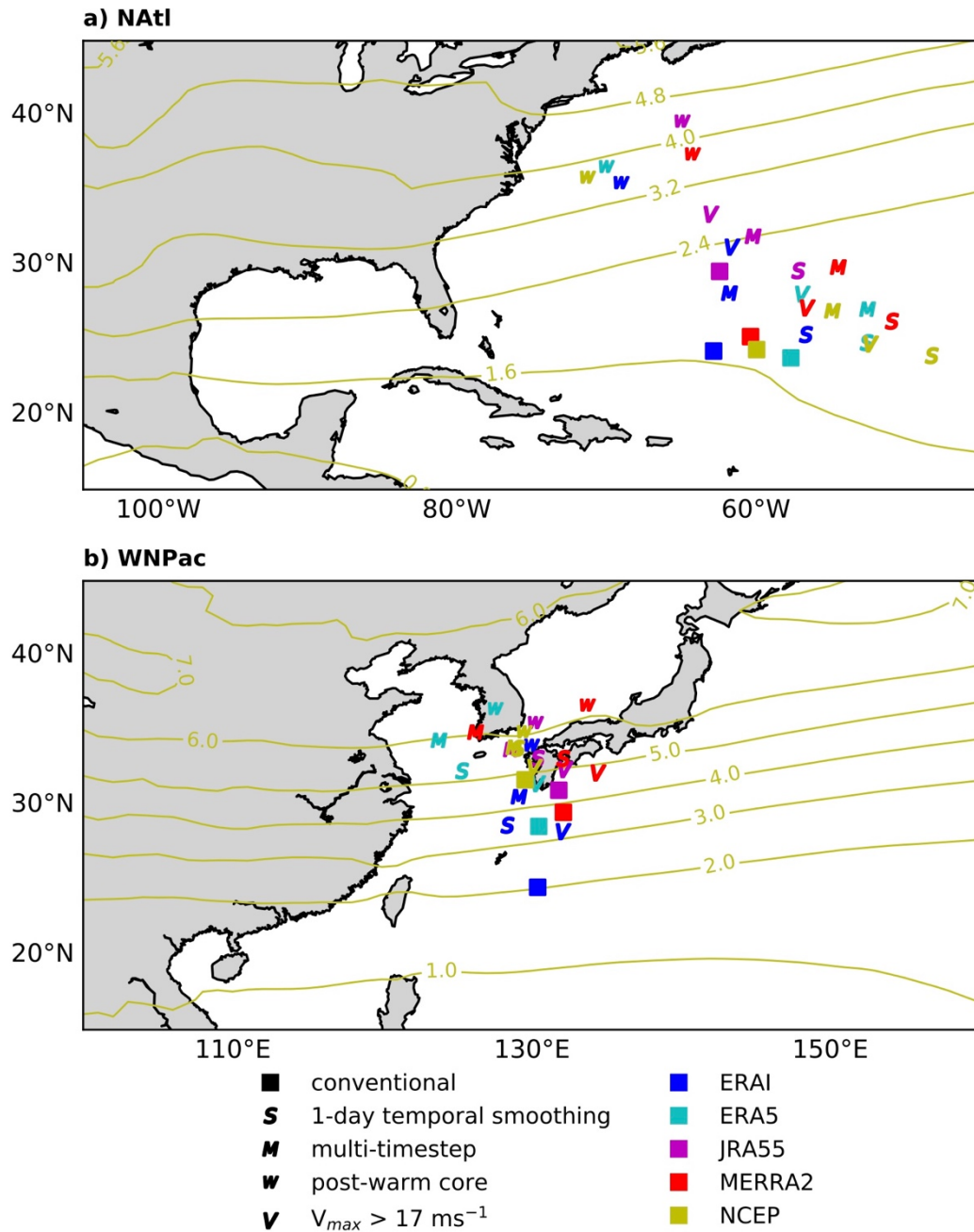

Fig. S2. Sensitivity of ET-completion location in reanalyses to published methodological approaches. Results are shown for (a) the North Atlantic ('NAtl') and (b) the Western North Pacific ('WNPac'). 'Conventional' (square markers) refers to the commonly used definition of ET completion: the first timestep at which both B and T_L indicate an extratropical structure. The other markers indicate a single modification of this definition. 'S': a 24-hour temporal smoothing of B and T_L trajectories was applied. 'M': ET completion is only identified where B and T_L criteria are satisfied for four consecutive timesteps. 'V': ET completion is only

identified for storms whose lifetime-maximum intensity exceeds 17 ms^{-1}. 'WC': a warm core lasting for at least two days is first identified for each storm and ET completion is identified thereafter. Overlain are contours of climatological-mean Eady growth rate maxima for August–November in units of day^{-1}, computed using ERA5 wind and geopotential data using Eq. 4.
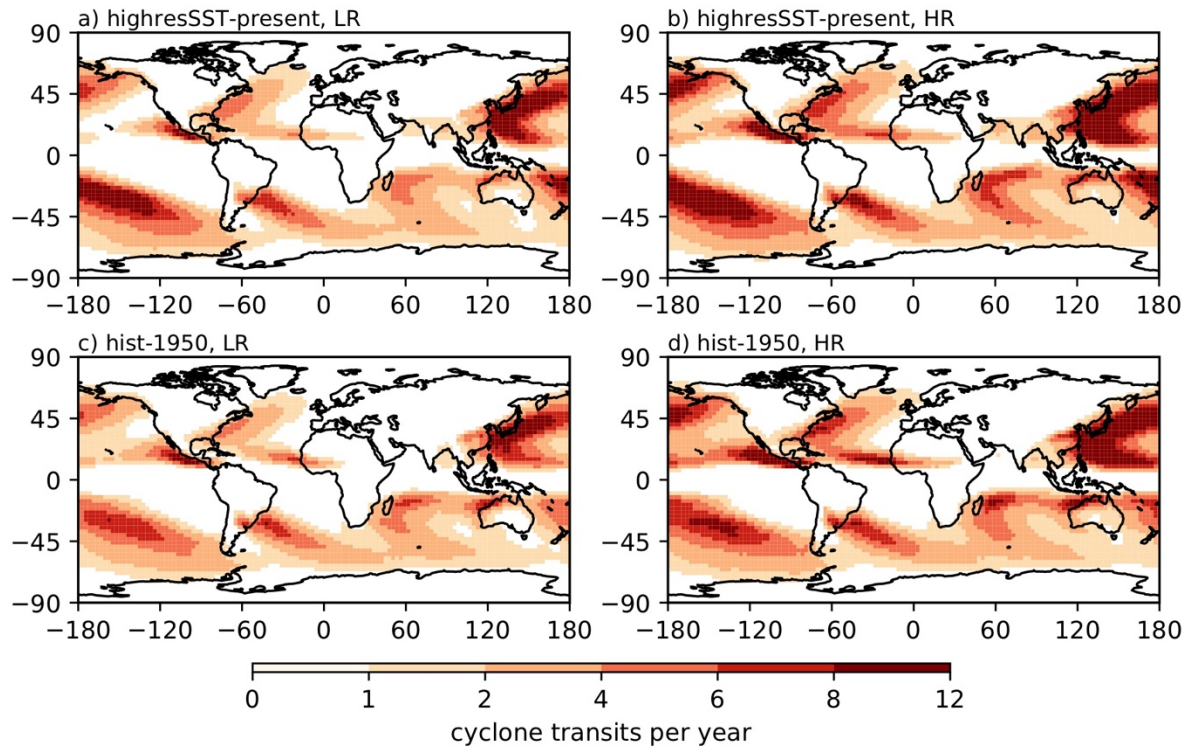
Fig. S3. Historical ensemble-mean track density simulated in low- and high-resolution (a–b) *highresSST-present* and (c–d) *hist-1950* experiments. Unit is cyclone transits per year per unit area (within a 5º geodesic radius of storm centres). Colour scale is the same as in Fig. 1a.
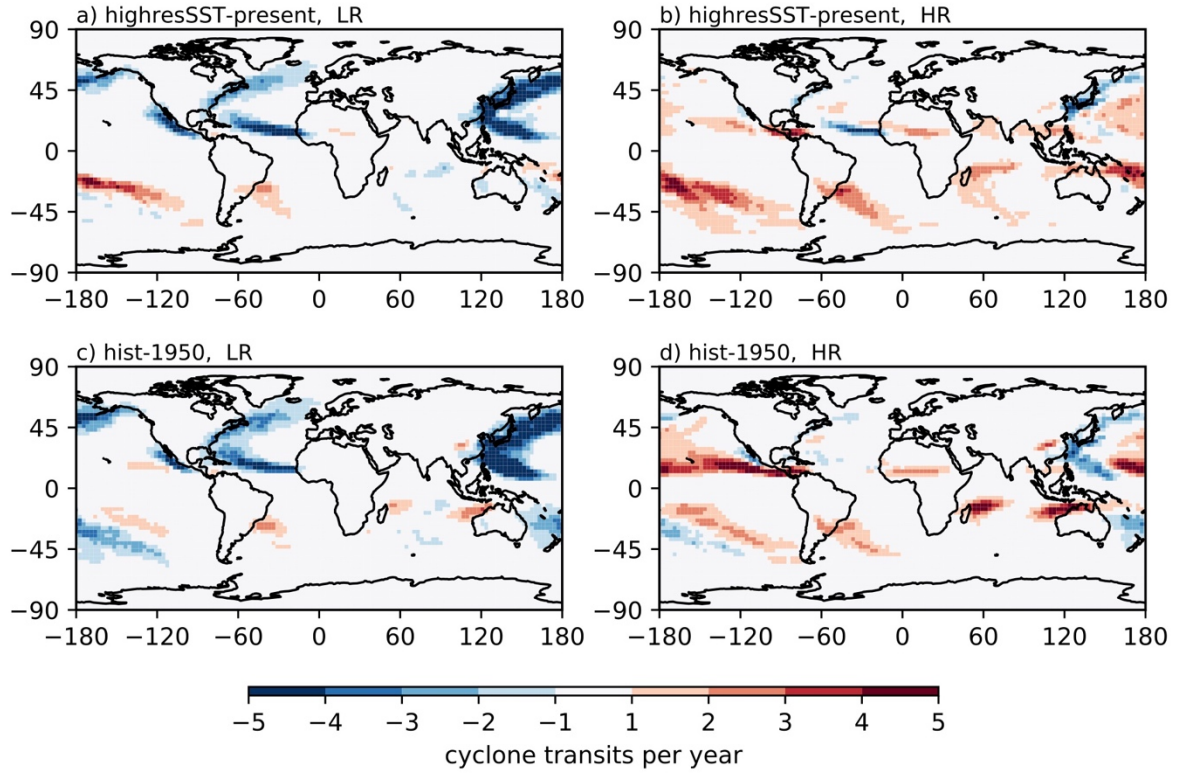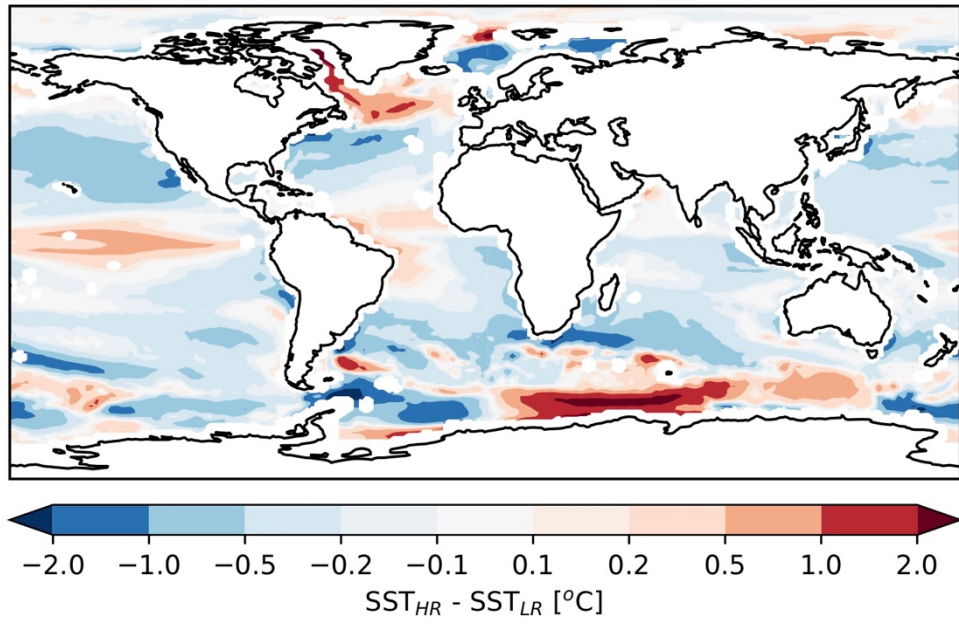
Fig. S4. Historical ensemble-mean track density biases (compared with multireanalysis-mean track density) simulated in low- and high-resolution (a–b) *highresSST-present* and (c–d) *hist-1950* experiments. Unit is cyclone transits per year per unit area (within a 5º geodesic radius of storm centres). Colour scale is the same as in Fig. 1c, e.

Fig. S5. Historical ensemble-mean August-November SST difference between low- and high-resolution *hist-1950* simulations. The low- and high-resolution sub-ensembles correspond to those of Fig. 1. Note the non-linear colour scale.
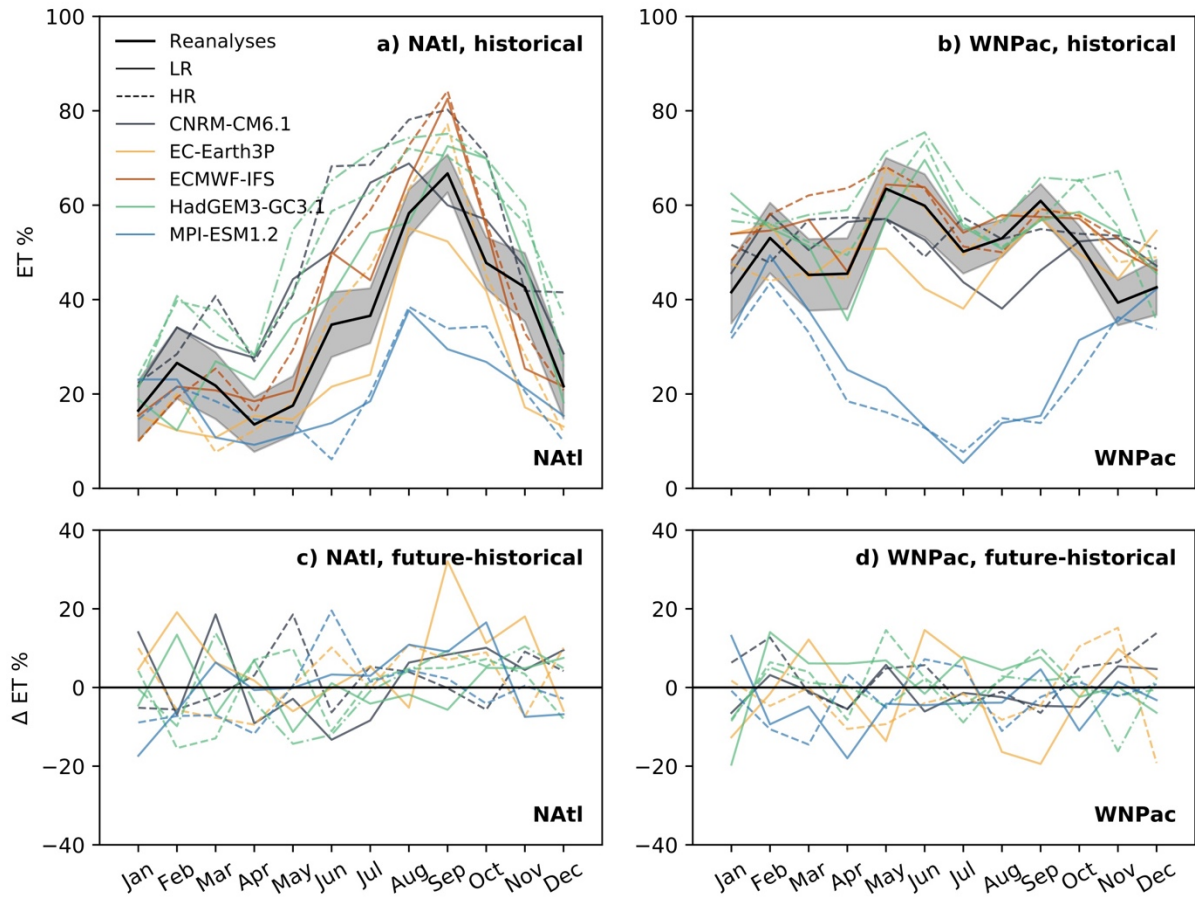
Fig. S6. Historical seasonal cycle of ET % in the (a) North Atlantic and (b) Western North Pacific basins. Shown are the multireanalysis mean (black with shading indicating standard error) and low- (solid) and high-resolution (dashed) *highresSST-present* simulations. (c–d) The difference between the future and historical seasonal cycles in ET % (i.e., *highresSST-future* minus *highresSST-present*). HadGEM3-GC3.1-MM is indicated by the dot-dashed line.
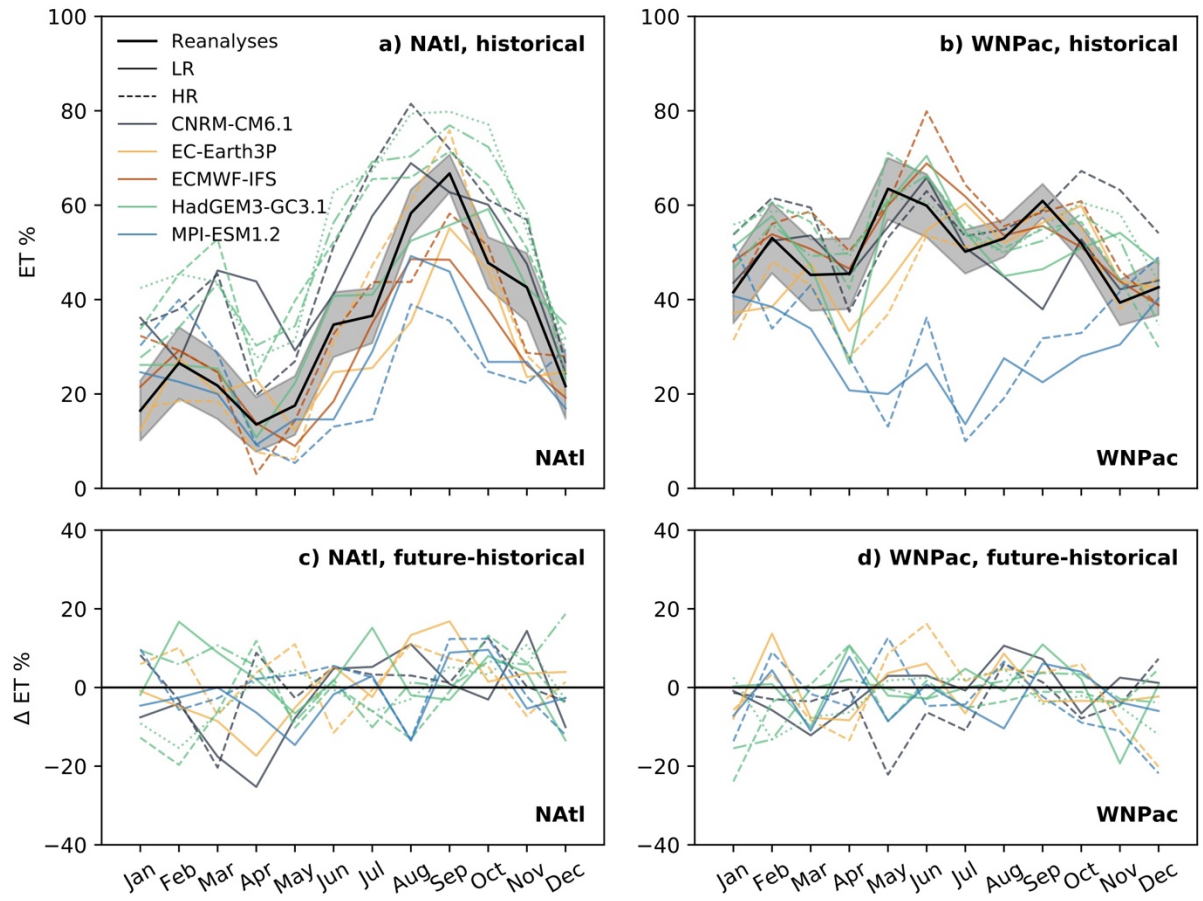
Fig. S7. Same as Fig. S6 but for fully coupled simulations. HadGEM3-GC3.1-MM and -HH are indicated by the dot-dashed and dotted lines, respectively.
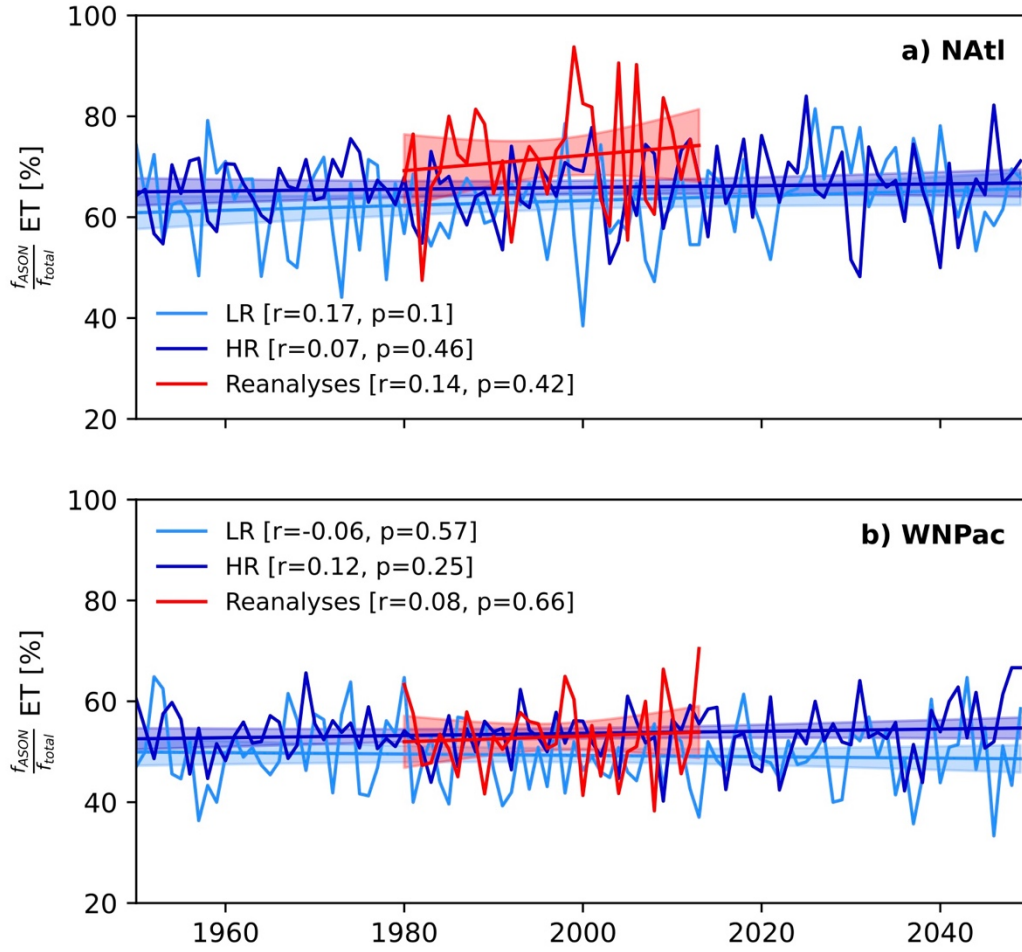
Fig. S8. Secular change in the ensemble-mean proportion of ET events occurring during August–November in reanalyses (red) and in low- (pale blue) and high-resolution (dark blue) fully coupled simulations for (a) the North Atlantic and (b) the Western North Pacific basins. Shading shows the 95 % confidence interval for the linear fit. ECMWF-IFS is not included in this analysis because no future simulations were performed in HighResMIP for this model.